THE GEOLOGICAL SOCIETY OF AMERICA®

A new Alpine geo-lithological map (Alpine-Geo-LiM) and global carbon cycle implications

Marco Donnini[1,†], Ivan Marchesini[1], and Azzurra Zucchini[2]
[1]*Istituto di Ricerca per la Protezione Idrogeologica, Consiglio Nazionale delle Ricerche (CNR), I-06128 Perugia, Italy*
[2]*Dipartimento di Fisica e Geologia, Università degli Studi di Perugia, I-06123 Perugia, Italy*

ABSTRACT

The chemical composition of river waters gives a measure of the atmospheric CO_2 fixed by chemical weathering processes. Since the dominating factors controlling these processes are lithology and runoff, as well as uplift and erosion, we introduce a new simplified geo-lithological map of the Alps (Alpine-Geo-LiM) that adopted a lithological classification compliant with the methods most used in literature for estimating the consumption of atmospheric CO_2 by chemical weathering. The map was used together with published alkalinity data of the 33 main Alpine rivers (1) to investigate the relationship between bicarbonate concentration in the sampled waters and the lithologies of the corresponding drained basins, and (2) to quantify the atmospheric CO_2 consumed by chemical weathering. The analyses confirm (as known by the literature) that carbonates are lithologies highly prone to consuming atmospheric CO_2. Moreover, the analyses show that sandstone (which could have a nonnegligible carbonate component) plays an important role in consuming atmospheric CO_2. Another result is that in multilithological basins containing lithologies more prone to consuming atmospheric CO_2, the contribution of igneous rocks to the atmospheric CO_2 consumption is negligible. Alpine-Geo-LiM has several novel features when compared with published global lithological maps. One novel feature is due to the attention paid in discriminating metamorphic rocks, which were classified according to the chemistry of protoliths. The second novel feature is that the procedure used for the definition of the map was made available on the Web to allow the replicability and reproducibility of the product.

INTRODUCTION

Carbon is the fourth most abundant element in the universe (Morgan and Anders, 1980; Anders and Ebihara, 1982), and it plays a vital role in Earth's environment. This element migrates continuously among four sinks: oceans, atmosphere, ecosystems, and geosphere (Holland, 1978; Berner, 2003; Kump et al., 2009). Considering the time scale of the phenomena, the "short-term" carbon cycle (shorter than 1 m.y.) is distinguished from the "long-term" carbon cycle (longer than 1 m.y.). The 1 m.y. threshold is assumed in literature to be coherent with the residence time of Ca^{2+} in the ocean system (Donnini et al., 2016). In the "short-term" carbon cycle, carbon is rapidly exchanged within surficial systems, such as oceans, biosphere, soil, and atmosphere, where the anthropogenic CO_2 production is also taken into account. In the "long-term" carbon cycle, carbon is slowly exchanged between the geosphere and the ocean-atmosphere system. Here, the concentration of atmospheric CO_2 mainly derives from the balance between the CO_2 produced by both volcanism and metamorphism, and the atmospheric CO_2 consumed by weathering of silicates and carbonates (Berner et al., 1983; Berner, 1991, 1994, 2004, 2006; Berner and Kothavala, 2001; Gislason and Oelkers, 2011; Li and Elderfield, 2013).

Because the solutes produced by chemical weathering enrich the river dissolved load, the composition of river waters can be considered as a good indicator of chemical weathering processes (Mackenzie and Garrels, 1966; Garrels and Mackenzie, 1971; Meybeck, 1987; Tardy, 1986; Probst, 1992; Gaillardet et al., 1999; Viers et al., 2007; Berner and Berner, 2012). Starting with knowledge of both the chemical compositions and flow rates of river waters, as well as of the lithologies of their basins, two different methods can be used to calculate the atmospheric CO_2 consumed by chemical weathering (Hartmann, 2009; Hartmann et al., 2009): (1) the reverse and the (2) forward methods. Both methods assume that the only reactions occurring within the river basins are the alteration of silicates and the alteration of carbonates due to the presence of carbonic acid.

The reverse method uses mass balance equations to discriminate weathering products by considering specific lithological end members (Garrels and Mackenzie, 1967; Meybeck, 1987; Gaillardet et al., 1999). Consequently, the stoichiometric relationships between the cations dissolved in the fluvial waters give, with good approximation, an estimate of the moles of atmospheric CO_2 involved in the alteration processes (Probst et al., 1994; Amiotte-Suchet, 1995; Amiotte-Suchet and Probst, 1996; Boeglin and Probst, 1998; Mortatti and Probst, 2003; Donnini et al., 2016). Depending on the time scales, different reactions have to be considered in order to quantify the atmospheric CO_2 consumed by chemical weathering (Huh, 2010; Donnini et al., 2016).

The forward method assumes that lithology and runoff (i.e., the discharge per unit area) are the predominant controlling factors of bicarbonate concentration in river waters, which is a measure of the atmospheric CO_2 consumed by chemical weathering. For specific lithologies, the runoff is linked to the atmospheric CO_2 consumed by chemical weathering through empirical relationships. In this way, it is possible to quantify the atmospheric CO_2 consumed by chemical weathering (Bluth and Kump, 1994; Amiotte-Suchet and Probst, 1993a, 1993b, 1995; Probst et al., 1994; Amiotte-Suchet et al., 2003; Hartmann, 2009; Hartmann et al., 2009).

A good understanding of the nature of the rocks is fundamental for building the empirical relationships between CO_2 consumption and lithology. As highlighted by Amiotte-Suchet et al. (2003) and by Moosdorf et al. (2010), geological maps often give scarce information regarding the chemical and physical nature of the rocks, focusing on the age of rocks, their deformation, their stratigraphy, and their structural position. This lack of information is problematic, especially for sedimentary rocks, which are very abundant in orogens (Doglioni, 1994;

†marco.donnini@irpi.cnr.it.

GSA Bulletin; September/October 2020; v. 132; no. 9/10; p. 2004–2022; https://doi.org/10.1130/B35236.1; 6 figures; 8 tables; Data Repository item 2020085.
published online 4 February 2020

Einsele et al., 1996; Clift et al., 2001) and which have a highly variable chemical composition (Amiotte-Suchet et al., 2003). Moreover, it is often not simple to obtain information about the protoliths of metamorphic rocks.

In the literature, a few lithological maps have been published at the global scale and are illustrated in the following. Gibbs and Kump (1994) presented a $2° \times 2°$ global lithological map classified into the six following rock types: (1) carbonates, (2) shales, (3) sandstones, (4) extrusive igneous rocks, (5) shield areas (including both intrusive igneous rocks and metamorphic rocks), and (6) "complicated lithology" (where it was difficult to discern a single rock type within the $2° \times 2°$ grid cell). That lithological map was used together with a derived $7.5° \times 4.5°$ global runoff map to calculate the global riverine bicarbonate flux by using the relationships between runoff and bicarbonate flux from Bluth and Kump (1994).

Amiotte-Suchet and Probst (1995) elaborated a $1° \times 1°$ global map of CO_2 consumption (Global Erosion Model for CO_2 fluxes [GEM-CO_2]) starting from the simplified lithological and soil maps published by the Food and Agriculture Organization (FAO) and United Nations Educational, Scientific and Cultural Organization (UNESCO) (FAO-UNESCO, 1971, 1975, 1976, 1978, 1979, 1981) and exploiting the relationships estimated by Meybeck (1986) considering more than 200 French monolithological basins (Amiotte-Suchet and Probst, 1993a, 1993b). Amiotte-Suchet and Probst (1995) defined the total atmospheric/soil CO_2 flux consumed by rock weathering, $\phi(CO_2)_{short}$, as the CO_2 moles consumed per area unit in a given period of time. In the map, the following seven lithologies were considered: (1) plutonic and metamorphic rocks, (2) sand and sandstone, (3) acid volcanic rocks, (4) evaporite rocks, (5) basalts, (6) shales, and (7) carbonate rocks.

Subsequently, Amiotte-Suchet et al. (2003) elaborated a $1° \times 1°$ global lithological map considering six rock categories: (1) sands and sandstone, (2) shales, (3) carbonate rocks, (4) combined intrusive igneous rocks and metamorphic rocks (i.e., shield rocks), (5) acid volcanic rocks, and (6) basalts. Compared with the map presented by Gibbs and Kump (1994), the map of Amiotte-Suchet et al. (2003) has a greater resolution ($1° \times 1°$ vs. $2° \times 2°$), and it is more informative, since ~27% of the total exposures are "complicated lithology" in the map of Gibbs and Kump (1994), and, as such, they are not precisely characterized (Amiotte-Suchet et al., 2003). Similar to Amiotte-Suchet and Probst (1995), $\phi(CO_2)_{short}$ was estimated by Amiotte-Suchet at al. (2003) through the relationship between $\phi(CO_2)_{short}$ and runoff published by Meybeck (1986).

A more detailed global lithological map was published by Dürr et al. (2005) at 1:25,000,000 scale. In contrast to the maps published by Gibbs and Kump (1994) and by Amiotte-Suchet et al. (2003), which are two grid-based raster maps, the map of Dürr et al. (2005) is in vector format and includes 8300 polygons. The map considers 15 rock categories (excluding water and ice): (1) acid volcanic rocks, (2) basic volcanic rocks, (3) acid plutonic rocks, (4) basic plutonic rocks, (5) Precambrian basement, (6) metamorphic rocks, (7) consolidated siliciclastic rocks, (8) mixed sedimentary rocks, (9) carbonates, (10) semi- to unconsolidated sedimentary rocks, (11) alluvial deposits, (12) loess, (13) dunes, (14) evaporites, and (15) complex lithology (where sediments, volcanic, and metamorphic rocks are mixed together). Together with outcropping lithologies, the map contains three other thematic layers containing other geological information (major subsurface evaporite occurrences, geology, and limits of maximum Quaternary glaciation extent).

Another global lithological map (named GLiM), in vector format, was presented by Hartmann and Moosdorf (2012). The map includes 1,235,400 polygons at 1:1,000,000 scale. Following Moosdorf et al. (2010), the map contains three levels of information (layers). The first one is mandatory and represents the general lithology. It considers 15 lithologies (excluding water and ice): (1) evaporites, (2) metamorphics, (3) acid plutonic rocks, (4) basic plutonic rocks, (5) intermediate plutonic rocks, (6) pyroclastics, (7) carbonate sedimentary rocks, (8) mixed sedimentary rocks, (9) siliciclastic sedimentary rocks, (10) unconsolidated sediments, (11) acid volcanic rocks, (12) basic volcanic rocks, (13) intermediate volcanic rocks, (14) Precambrian rocks, and (15) complex lithologies. The second and the third layers optionally contain information on the specific rock attributes.

At regional scale, Donnini et al. (2016) presented a lithological map of the Alps. The map was used, together with the major-element concentrations of the 33 main Alpine river waters, to estimate the atmospheric CO_2 consumption by chemical weathering in the Alpine region by applying the MEGA geochemical code (Amiotte-Suchet, 1995; Amiotte-Suchet and Probst, 1996), which implements the reverse method. This map was elaborated at 1:1,000,000 scale and considers eight lithological classes: (1) acid igneous rocks, (2) mixed carbonate, (3) clay and claystone, (4) debris, (5) mafic rocks, (6) metamorphic rocks, (7) pure carbonate rocks, and (8) sandstone.

In this paper, we introduce a new high-resolution (1:1,000,000 scale) simplified geo-lithological map of the Alps (named Alpine-Geo-LiM) that adopted a lithological classification (10 lithological classes: (1) "pure carbonate," (2) "mixed carbonate," (3) "gypsum evaporite," (4) "acid rocks," (5) "mafic rocks," (6) "intermediate rocks," (7) "sandstone," (8) "claystone," (9) "metamorphic rocks," and (10) "peats"), compliant with the reverse and the forward methods. Alpine-Geo-LiM was derived from the national geological maps of Italy, France, Germany, Switzerland, Austria, and Slovenia, and it represents an implementation of the map previously published in Donnini et al. (2016). Moreover, it is released together with the code adopted for building the map (Donnini et al., 2018). Although we used the same input data as in Donnini et al. (2016), Alpine-Geo-LiM differs from the map published in Donnini et al. (2016) in the lithological classification, i.e., eight lithological classes of Donnini et al. (2016) versus 10 lithological classes for Alpine-Geo-LiM, as well as in a more accurate analysis of the protoliths of metamorphic rocks. Moreover, unlike Donnini et al. (2016), Alpine-Geo-LiM is released in vector format together with both the informatic procedures used to elaborate the map and the original data (see Donnini et al., 2018). We define Alpine-Geo-LiM as a geo-lithological map since we provide the lithological map, but we also provide the original layers and procedure used to create the map. Moreover, we release, in the attribute table, the original geological information (Appendixes A, B, and C[1]).

Alpine-Geo-LiM, together with the alkalinity of the 33 main Alpine rivers sampled in 2011 and 2012 (Donnini et al., 2016), was used: (1) to investigate the relationship between HCO_3^- concentration in the sampled river waters and the lithologies of the corresponding drainage basins, and, applying the forward method, (2) to quantify the atmospheric CO_2 consumed by chemical weathering.

STUDY AREA

The Alps (south-central Europe; Fig. 1) are a collisional belt generated by the Cretaceous to present convergence of the European and African (also named Adriatic or Apulian) continental margins, which caused the closure of

[1]GSA Data Repository item 2020085, Appendix A: Deep description of the geology of the Alps; Appendix B: Names of the attribute fields of the different national geological maps used for the elaboration of Alpine-Geo-LiM; Appendix C: Considerations done to classify some specific Alpine geological units, is available at http://www.geosociety.org/datarepository/2020 or by request to editing@geosociety.org.

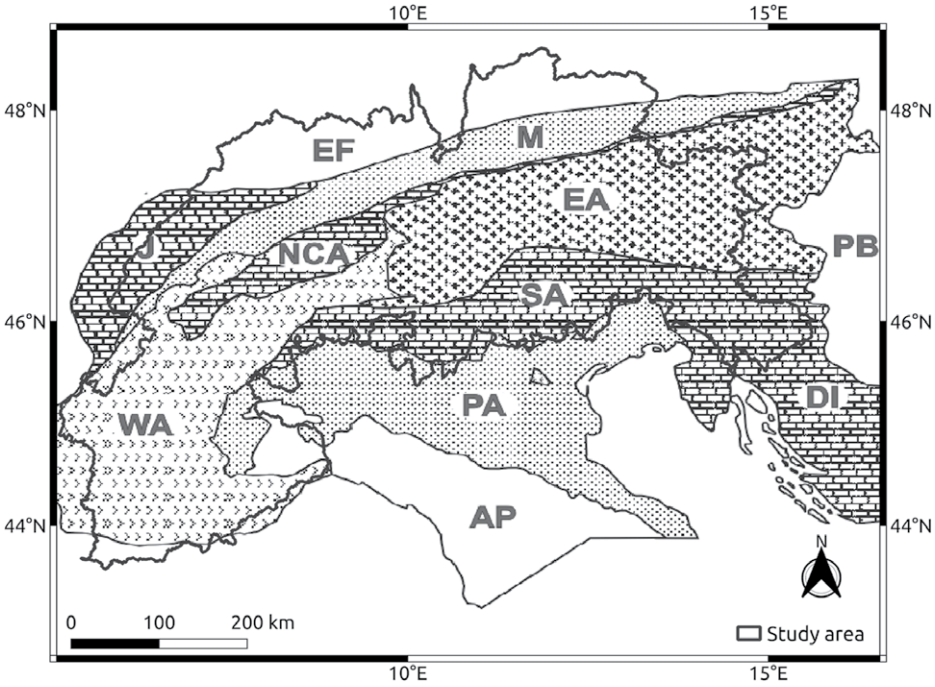

Figure 1. Hydrogeological map of the Alps (modified from Rossi and Donnini, 2018). WA—western Alps, EA—eastern Alps, NCA—Northern Calcareous Alps, SA—southern Alps, J—Jura Mountains, AP—Apennines, DI—Dinarides, M—Molasse Basin, PA—Po Valley and Adriatic foreland, PB—Pannonian Basin, EF—European foreland.

the ocean located in the Mediterranean region (Trümpy, 1960; Frisch, 1979; Tricart, 1984; Haas et al., 1995; Stampfli et al., 2001; Dal Piaz et al., 2003; Schmid et al., 2004; Pfiffner, 2014).

The Alps have an arc shape and can be roughly subdivided into the following different geological domains (Dal Piaz et al., 2003; Schmid et al., 2004; Pfiffner, 2014) shown in Figure 1: the eastern Alps, the Northern Calcareous Alps, the southeastern Eoalpine Calcareous Alps, and the western Alps. The Alps are partially continuous to the northwest with the Apennine chain and to the east with the Dinarides. The Pannonian basin bounds the Alps to the east, the Molasse Basin bounds the Alps to the north, and the Po Valley and Adriatic foreland bound the chain to the south. The Jura Mountains define the northwestern boundary of Alps. External to the Alps, in the north, there is the European foreland. The polygon in Figure 1 represents the study area, corresponding to the subdivision of the Alps into the 33 main Alpine river basins used by Donnini et al. (2016).

The geology of the Alps can be roughly schematized using the following geological domains (Rossi and Donnini, 2018): (1) Austroalpine crystalline rocks in the eastern Alps; (2) carbonate rocks in the Jura Mountains, in the Northern Calcareous Alps, and in the southeastern Eoalpine Calcareous Alps; and (3) Helvetic calcareous units mixed with crystalline massifs and Penninic metamorphic-ophiolitic units in the western Alps. Outside of the Alpine chain, (1) the Molasse basin in the north is filled by Tertiary successions having several kilometers of thickness, and (2) the Po Valley and Adriatic foreland in the south mainly consist of alluvial deposits, as do the Pannonian basin and the European foreland.

From a geomorphologic point of view, the Alps are characterized by altitudes ranging between 1200 and 1300 m above sea level (m.a.s.l.), extensive lowlands, deeply incised valleys, and mountains higher than 4000 m.a.s.l. (the highest peak is Monte Bianco at 4888 m.a.s.l.; Dal Piaz et al., 2003), leading to a strong topographic variability (Carraro and Giardino, 2004; Gobiet et al., 2014).

Temperature extremes and annual precipitation are related to the physiography of the Alps. The valley bottoms are generally warmer and drier than the surrounding mountains. In winter, nearly all precipitation above 1500 m.a.s.l. is in the form of snow. Snow cover lasts from approximately mid-November to the end of May at 2000 m.a.s.l (Diem et al., 2019). The precipitation stored as snow and ice in the winter season is released in the following months after their fusion (European Environmental Agency, 2010). The water in the Alpine region is in the form of lakes, aquifers, and glaciers, which feed many basins in Europe, including the Rhine, Danube, Po, and Rhone (Weingartner et al., 2007), which are the biggest European rivers in terms of flow rate and basin area. Glaciers cover an area of ~2050 km^2 (Paul et al., 2011), representing 1% of the area of the 33 main Alpine basins (Donnini et al., 2016).

METHODS AND DATA

The following sections introduce the reader to (1) the basic equations governing atmospheric CO_2 consumption and (2) the new Alpine-Geo-LiM.

Weathering Estimation

The chemical composition of river waters is an indicator of weathering processes (Mackenzie and Garrels, 1966; Garrels and Mackenzie, 1971; Meybeck, 1987; Tardy, 1986; Probst, 1992; Gaillardet et al., 1999; Viers et al., 2007; Berner and Berner, 2012), which contribute, together with atmospheric input (rain), pollution, biota, and evaporite dissolution, to the dissolved load (e.g., Gaillardet et al., 1999; Galy and France-Lanord, 1999; Roy et al., 1999; Moon et al., 2007; Wu et al., 2008; Gao et al., 2009; Jha et al., 2009; Donnini et al., 2016). Weathering reactions of silicate minerals, hydrolysis, and carbonate dissolution consume atmospheric/soil CO_2 and produce an increase in the solution alkalinity. The forward reactions of silicate and carbonate alteration by carbonic acid are the only reactions that occur within the river basins in the "short-term" and are described by the following equations (Mortatti and Probst, 2003; Donnini et al., 2016):

albite into kaolinite:

$$2NaAlSi_3O_8 + 2CO_2 + 11H_2O \leftrightarrows Al_2Si_2O_5(OH)_4 + 2HCO_3^- + 2Na^+ + 4H_4SiO_4, \quad (1)$$

K-feldspar into montmorillonite:

$$2KAlSi_3O_8 + 2CO_2 + 6H_2O \leftrightarrows Al_2Si_4O_{10}(OH)_2 + 2HCO_3^- + 2K^+ + 2H_4SiO_4, \quad (2)$$

Ca-plagioclase into kaolinite:

$$CaAl_2Si_2O_8 + 2CO_2 + 3H_2O \rightarrow Al_2Si_2O_5(OH)_4 + 2HCO_3^- + Ca^{2+}, \quad (3)$$

olivine weathering:

$$Mg_2SiO_4 + 4CO_2 + 4H_2O \rightarrow 2Mg^{2+} + 4HCO_3^- + H_4SiO_4, \quad (4)$$

calcite dissolution:

$$CaCO_3 + CO_2 + H_2O \leftrightarrows Ca^{2+} + 2HCO_3^-, \quad (5)$$

dolomite dissolution:

$$CaMg(CO_3)_2 + 2CO_2 + 2H_2O \leftrightarrows Ca^{2+} + Mg^{2+} + 4HCO_3^-. \quad (6)$$

In the "long-term" period, not all the atmospheric CO_2 is permanently removed by weathering reactions because some of the carbon is returned to the atmosphere (Huh, 2010; Donnini et al., 2016). In particular, the rivers' dissolved load released to the oceans is partially precipitated as carbonate (mainly reverse reaction in Eq. 5) or authigenic clays (reverse reactions in Eq. 1 and Eq. 2). In particular, Equation 5 shows that weathering of $CaCO_3$ consumes one unit of CO_2 (forward reaction, "short-term"), and that the same amount of CO_2 is returned to the atmosphere upon precipitation of $CaCO_3$ in the seas and/or oceans (reverse reaction, "long-term").

A similar behavior might be due to the weathering of $CaMg(CO_3)_2$ (see Eq. 6), where two units of CO_2 consumed by weathering (forward reaction, "short-term") return to the atmosphere upon precipitation of $CaMg(CO_3)_2$ in the seas and/or oceans (reverse reaction, "long-term"). However, the direct precipitation of dolomite at ambient temperature from aqueous solution is prevented (e.g., Frondini et al., 2014, and references therein) by a strong solvation shell of aqueous Mg^{2+} as well as by crystallization barriers that inhibit the formation of Ca-Mg ordered dolomite (Montes-Hernandez et al., 2016). Therefore, the reverse reaction of Equation 6 is just theoretically considered.

Weathering reactions of silicate minerals containing Na and K (albite and K-feldspar) consume atmospheric CO_2 (Eq. 1 and Eq. 2 forward reactions, "short-term"). When Na^+ and K^+ ions are transported by rivers to the oceans and/or seas, they could be subjected to reverse weathering, forming authigenic clays and releasing atmospheric CO_2 (Eq. 1 and Eq. 2 reverse reactions, "long-term"; Huh, 2010).

Equation 3 and Equation 4 are not reversible, and the products of the forward reactions (HCO_3^-, Ca^{2+}, and Mg^{2+}) are involved in the reverse reactions described by Equation 5. In particular, half of the units of atmospheric CO_2 consumed during weathering of Ca-plagioclase (Eq. 3) are precipitated in the oceans as $CaCO_3$ (according to Eq. 5, reverse reaction). The same might also occur for the product of the forward reaction of olivine (Eq. 4), when considering the reverse reaction of Equation 6. However, the last speculation is just theoretically given, as previously explained. The assumption that Equations 1–6 are the only reactions that occur in the river basins is valid (a) if carbonic acid (H_2CO_3, derived from the interaction between river water and atmospheric CO_2) is the only source of protons in weathering reactions (the contribution of other acids [HNO_3, H_2SO_4] is negligible; Mortatti and Probst, 2003; Donnini et al., 2016), and (b) if pyrite (FeS_2), gypsum ($CaSO_4 \cdot 2H_2O$), and halite (NaCl) percentages are negligible in the river basins, and their dissolution is not considered in the model calculation (Perrin et al., 2008). Overall, the described conditions are valid in nonpolluted areas, for temperate climates, and for lithologies without pyrite.

As previously stated, two different methods were used to calculate the atmospheric CO_2 consumed by chemical weathering (Hartmann, 2009; Hartmann et al., 2009): (1) the reverse and the (2) forward method. In the following, a brief description of both approaches is reported.

Reverse Method

In the reverse method, the moles of atmospheric/soil CO_2 consumed by chemical weathering are computed from Equations 1–6, considering the forward ("short-term") and the reverse ("long-term") reactions. In practice, the measured dissolved cations in river waters are used to estimate the moles of consumed atmospheric/soil CO_2.

In the "short-term" (forward reactions), one mole of atmospheric CO_2 is consumed by the weathering of silicate minerals containing Na and K (Eq. 1 and Eq. 2) and carbonate minerals containing Ca and Mg (Eq. 5 and Eq. 6), whereas 2 moles of atmospheric CO_2 are consumed by silicate minerals containing Ca and Mg (Eq. 3 and Eq. 4). As a consequence, $\phi(CO_2)_{short}$ can be calculated by the following equation:

$$\phi(CO_2)_{short} = \phi(Na + K)_{sil} + 2\phi(Ca + Mg)_{sil} + \phi(Ca + Mg)_{carb}. \quad (7)$$

On the other hand, considering the "long-term" period, the total atmospheric/soil CO_2 flux consumed by rock weathering on a river basin, $\phi(CO_2)_{long}$, takes into account the CO_2 released to the atmosphere by precipitation of carbonates and authigenic clays due to the reverse reactions (Eqs. 1, 2, 5 and 6). As a consequence, only the weathering of silicate minerals containing Ca and Mg is a net sink for atmospheric/soil CO_2 (Huh, 2010; Berner et al., 1983; Donnini et al., 2016), and $\phi(CO_2)_{long}$ is given by:

$$\phi(CO_2)_{long} = \phi(Ca + Mg)_{sil}. \quad (8)$$

In Equation 7 and Equation 8, $\phi(X + Y)$ is the sum of the fluxes of two generic chemical species X and Y in river waters, given by its molar concentration multiplied by the runoff, while the suffixes "sil" and "carb" indicate the considered chemical species derived from either silicate or carbonate weathering (Huh, 2010; Donnini et al., 2016). Starting from the measured concentration of Ca^{2+} and Mg^{2+} in river waters, the contributions of silicate weathering, $(Ca + Mg)_{sil}$, and carbonate dissolution, $(Ca + Mg)_{carb}$, to the total riverine fluxes can be distinguished by using specific ionic ratios of water drained from monolithological basins (e.g., Meybeck, 1986, 1987).

The reverse method has been already applied by many authors to estimate the atmospheric CO_2 consumption in the Congo, Amazon, and Niger watersheds and in the 33 main Alpine river basins (Probst et al., 1994; Amiotte-Suchet, 1995; Amiotte-Suchet and Probst, 1996; Boeglin and Probst, 1998; Gaillardet et al., 1999; Mortatti and Probst, 2003; Moon et al., 2007; Donnini et al., 2016).

Forward Method

In the forward method, the moles of atmospheric/soil CO_2 consumed by chemical weathering are computed from Equations 1–6 considering only the "short-term" forward reactions.

The forward method assumes that, at the catchment scale, the amount of atmospheric/soil CO_2 consumed by chemical weathering on the "short-term" can be estimated from the bicarbonate concentration in river waters. The moles of atmospheric CO_2 consumed by chemical weathering are considered to be equivalent to the total moles of HCO_3^- in rivers draining silicate rocks (see Eqs. 1, 2, 3 and 4) and to half of the moles of HCO_3^- in rivers draining carbonate rocks (see Eqs. 5 and 6; Amiotte-Suchet and Probst, 1993a, 1993b, 1995; Probst et al., 1994; Amiotte-Suchet et al., 2003; Hartmann, 2009; Hartmann et al., 2009). The forward method does not consider the portion of carbon that returns to the atmosphere in the "long-term" period, and for this reason, it is applicable only to estimate the flux of atmospheric CO_2 consumed over the short-term according to the following equation:

$$\phi(CO_2)_{short} = \phi(HCO_3)_{sil} + \frac{1}{2}\phi(HCO_3)_{carb}. \quad (9)$$

Similar to Equation 7 and Equation 8, in Equation 9, $\phi(HCO_3)$ is the flux of moles of HCO_3^-, given by its molar concentration multiplied by the runoff. The suffixes "sil" and "carb" indicate whether the considered chemical species (HCO_3^-) derives from silicate or carbonate weathering.

In the literature, a set of empirical relationships links, for different lithologies, the flux of atmospheric/soil CO_2 consumed by chemical weathering on the "short-term," $\phi(CO_2)_{short}$, to the runoff. Amiotte-Suchet and Probst (1993a,

1993b, 1995), Probst et al. (1994), and Amiotte-Suchet et al. (2003) estimated the relationship between $\phi(CO_2)_{short}$ and runoff from the dissolved load and the runoff of more than 200 French monolithological river basins (Meybeck, 1986, 1987). Similar relationships were estimated by Bluth and Kump (1994) from the dissolved load and the runoff of ~100 monolithological catchments across the United States, Puerto Rico, and Iceland. In Hartmann (2009) and Hartmann et al. (2009), for the first time, the relationship between $\phi(CO_2)_{short}$ and runoff was estimated through a multivariate nonlinear regression analysis starting from 382 Japanese river basins draining more than one lithology.

The forward method considers that lithology and runoff are the dominating factors controlling the atmospheric CO_2 consumption processes, and that other factors, such as relief or land cover, are less important at both regional and global scale (Hartmann, 2009; Hartmann et al., 2009). A temperature dependence of the atmospheric CO_2 consumption is implemented only for the global basalt-weathering model (Dessert et al., 2003).

Starting from the empirical relationships between $\phi(CO_2)_{short}$ and runoff and knowing only the outcropping lithology and the runoff within a given territory, it is possible to estimate the moles of atmospheric CO_2 consumption. Data on the chemical composition of river water are not needed for this estimation. The forward model has been applied at basin scale in the Garonne, Congo, and Amazon River basins (Amiotte-Suchet and Probst, 1993a, 1993b, 1995; Probst et al., 1994), at regional scale in the Japanese Archipelago (Hartmann, 2009), and at a global scale (Amiotte-Suchet and Probst, 1995; Amiotte-Suchet et al., 2003; Hartmann et al., 2009).

Geological Maps

For the elaboration of our geographic information system (GIS)–based simplified geo-lithological map (1:1,000,000 scale) of the Alps, we took advantage of the geological layers, in vector format, extracted from (1) the geological map of Italy at 1:500,000 scale (Bonomo et al., 2006) released by the Italian Institute for Environmental Protection and Research (ISPRA; http://www.isprambiente.gov.it), (2) the geological map of Switzerland at 1:500,000 scale (Bundesamt für Landestopografie, 2005) released by the Swiss Federal Office of Topography (Swisstopo; http://www.swisstopo.admin.ch), (3) the geological map of Germany at 1:1,000,000 scale (BGR, 2011), (4) the geological map of Austria at 1:500,000 scale (Egger et al., 1999) released by the Geological Survey of Austria (GBA; http://www.geologie.ac.at), (5) the geological map of France at 1:1,000,000 scale (BRGM, 2003), and (6) the geological map of Slovenia at 1:250,000 scale (Buser, 2010). These two last maps were obtained from the European Geological Data Infrastructure (EGDI; http://www.europe-geology.eu/metadata). The six maps are released in ESRI shapefile formats having different coordinate reference systems and different accuracy and information quality. The layers of France, Germany, and Slovenia contained several topological errors (e.g., gaps between polygon borders, overlapping polygon borders, etc.) and were corrected by removing duplicate boundaries and areas smaller than, respectively, 1 m^2, 600 m^2, and 50 m^2 (the longest boundary with adjacent area was removed).

The attribute tables of the vector maps contain different attribute fields where the description of the geological information is stored. Those fields are listed in the Appendix B (see footnote 1).

Geo-lithological Classification Scheme

According to Moosdorf et al. (2010, p. 2), "classification is a constant compromise between exactness and simplicity." The lithological classification used in Alpine-Geo-LiM is a compromise among the 6–7 rock categories used by Gibbs and Kump (1994), Amiotte-Suchet and Probst (1995), and Amiotte-Suchet at al. (2003), and the 15 rock categories used by Dürr et al. (2005), Hartmann and Moosdorf (2012), and Moosdorf et al. (2010), since we consider the first classification too simplified and the second one too detailed. Ten lithologies were taken into account for Alpine-Geo-LiM: (1) "pure carbonate," (2) "mixed carbonate," (3) "gypsum evaporite," (4) "acid rocks," (5) "mafic rocks," (6) "intermediate rocks," (7) "sandstone," (8) "claystone," (9) "metamorphic rocks," and (10) "peats."

The "pure carbonate" category includes rocks composed mainly of calcite, aragonite ($CaCO_3$), and dolomite [$MgCa(CO_3)_2$], such as limestone, dolomite, and travertine, as well as marble, for which the protolith is composed by carbonate rock (Pettijohn, 1957; Garrels and Mackenzie, 1971; Boggs and Boggs, 2009).

The "mixed carbonate" category includes rocks composed of carbonate minerals mixed with noncarbonate minerals. In this category, there are impure carbonate rocks, calcarenites, and marls (Pettijohn, 1957).

In the "gypsum evaporite" category, we include gypsum and anhydrite. We know that, generally, the term evaporites refers to anhydrite, gypsum, and halite (Garrels and Mackenzie, 1971). However, since the analyzed bibliographic sources (see Appendixes A and C, and references therein [footnote 1]) excluded the presence of halite in the Alps, in this work only gypsum and anhydrite were included in the "gypsum evaporite" group.

The subdivision among "acid rocks," "mafic rocks," and "intermediate rocks" was done according to (1) the total-alkali-silica (TAS) diagram (Le Bas et al., 1986; Middlemost, 1994), which classifies many common types of volcanic rocks starting from the relationships between the combined alkali ($Na_2O + K_2O$) and silica (SiO_2) contents, and (2) an adaptation of the same diagram for plutonic rocks (Le Bas et al., 1986; Middlemost, 1994). Thus, we considered "mafic rocks" those with less than 50%–52% of SiO_2, "intermediate rocks" the rocks with SiO_2 content between 50%–52% and 60%–62%, and "acid rocks" those with more than 60%–62% of SiO_2. The metamorphic rocks, which are not included in the two TAS diagrams, were classified according to Mottana et al. (2009). Based on the compositions of the protoliths, an orthogneiss was considered as "acid rocks" (assuming a granitic protolith composition), and a serpentinite was considered as "mafic rocks" (Mottana et al., 2009).

In the "sandstone" category, we included arkose, graywacke (Garrels and Mackenzie, 1971), and conglomerate, the last one being similar to sandstone in terms of origin and depositional mechanisms (Boggs and Boggs, 2009). Moreover, the metamorphic rock quartzite falls in the "sandstone" category, as its protolith (Mottana et al., 2009).

In the "claystone" category, we included shale, argillite, siltstone, and mudstone (Garrels and Mackenzie, 1971; Boggs and Boggs, 2009), as well as, again considering the protoliths (Mottana et al., 2009), the metamorphic phyllite, schists, and paragneiss.

The generic "metamorphic rocks" category was used only when information on protoliths was unavailable or unclear (e.g., in the case of migmatite, mylonite, and metasediments).

Finally, we introduced the further lithology "peat," due to the presence of these types of deposits in the Alps.

Rocks composed by more than one lithotype posed some problems for their classification. Goldich (1938) introduced a weathering series of silicates that was further modified by Railsback (2006), who added some nonsilicate minerals. According to this weathering series, carbonate dissolution is considerably higher than silicate dissolution, whereas gypsum/anhydrite dissolution is higher than carbonate dissolution. For this reason, (1) in the "gypsum evaporite" category, we also included rocks composed of a mix of carbonate and gypsum/anhydrite, and (2) in the "mixed carbonate rocks" category, we also included the rocks composed of more than one lithotype, where at least one of them was composed of "mixed

carbonate rocks" (e.g., a lithotype composed by sandstone, graywacke, and marl was considered "mixed carbonate rocks").

For the silicate rocks composed by more than one lithotype, we adopted the "principle of prevalence." We classified these rock types according to the most abundant lithologies among those listed in the different fields of the reference map attribute tables. For example, an outcrop (a polygon of the vector map) where the different field attributes reported the presence of basalt, trachybasalt, and andesite was included in the "basic rocks" class, since, following our classification, basalt and trachybasalt can be considered as "basic rocks" and only andesite as is classified as "intermediate rocks."

In the rare occasions when an outcrop is composed by "intermediate rocks" and "acid rocks" (or "mafic rocks") in the same proportions, it was considered as "acid rocks" (or "mafic rocks"). This is the case, as an example, of an outcrop composed by monzonite ("intermediate rocks") and granite ("acid rocks"); it was considered as "acid rocks." An in-depth study of alpine geology, described in the Appendix C (see footnote 1), was carried out to classify specific geological units.

Alpine Geo-Lithological Map (Alpine-Geo-LiM)

The new Alpine-Geo-LiM is a portion of the "Geo-Lithological Map of Central Europe" (Geo-LiM; Donnini et al., 2018), which was released in vector format, and which is freely downloadable at the Web address (https://doi.org/10.5281/zenodo.3530257, Donnini et al., 2018). The map is composed by 12,001 polygons. Some very small polygons exist in the map (due to the cut of the map along the boundaries of the studied area). The biggest polygon has an area of ~11,197.5 km^2, and the average polygons size is ~16.5 km^2.

The preprocessing (cleaning of topological errors) and processing (unions, intersections, and classifications) steps to build the map were performed using GRASS GIS (Neteler and Mitasova, 2008; Neteler et al., 2012), an open-source GIS software, and PostgreSQL (PostgreSQL - http://www.postgresql.org), an open-source relational database management system (RDBMS), with its PostGIS spatial extension (PostGIS; http://www.postgis.org).

The attribute table of the resulting map is composed by the following 10 fields: *litho_irpi*, *rsil_mm*, *orig1*, *orig2*, *orig3*, *orig4*, *orig5*, *orig6*, *orig7*, and *country*. The *litho_irpi* field was compiled with one of the 10 aforementioned lithological classes ("acid rocks," "mafic rocks," "intermediate rocks," "metamorphic rocks," "sandstone," "claystone," "pure carbonate rocks," "mixed carbonate rocks," "gypsum evaporite," and "peat"). The *orig1*, *orig2*, *orig3*, *orig4*, *orig5*, *orig6*, and *orig7* fields contain the original geological information derived from the six original geological maps (Italy, Switzerland, Germany, Austria, France, Slovenia; see Appendix B [footnote 1]), and the *country* field contains the name of the country.

The command lines and queries used for building the map based on the original data are provided together with the geo-lithological map herein.

Lithology and Morphology of the Study Area

Alpine-Geo-LiM is shown in Figure 2. The colors used to distinguish the different lithologies in Alpine-Geo-LiM were derived from the lithologic legend adopted by the U.S. Geological Survey (USGS) for the geologic maps of the United States. The legend and the red-green-blue (RGB) codes are made available by the USGS on the Web (https://mrdata.usgs.gov/catalog/lithclass-color.php).

The abundance of rock types outcropping in the Alpine region is shown in Table 1, and it was estimated within an area of 197,773 km^2, corresponding to the area of the main Alpine river basins (Fig. 3) defined in Donnini et al. (2016). The table shows that carbonate rocks are the most abundant type in Alpine region, with 23.75% of "mixed carbonate" and 20.82% of "pure carbonate," for a total of 44.57%. They are followed by "sandstone" (26.99%), "claystone" (12.87%), and volcanic rocks (with 7.38% of "acid rocks," 2.69% of "mafic rocks," and 0.43% of "intermediate rocks," for a total of 10.50%). "Metamorphic rocks" represent 1.81% of the study area, while "peats" and

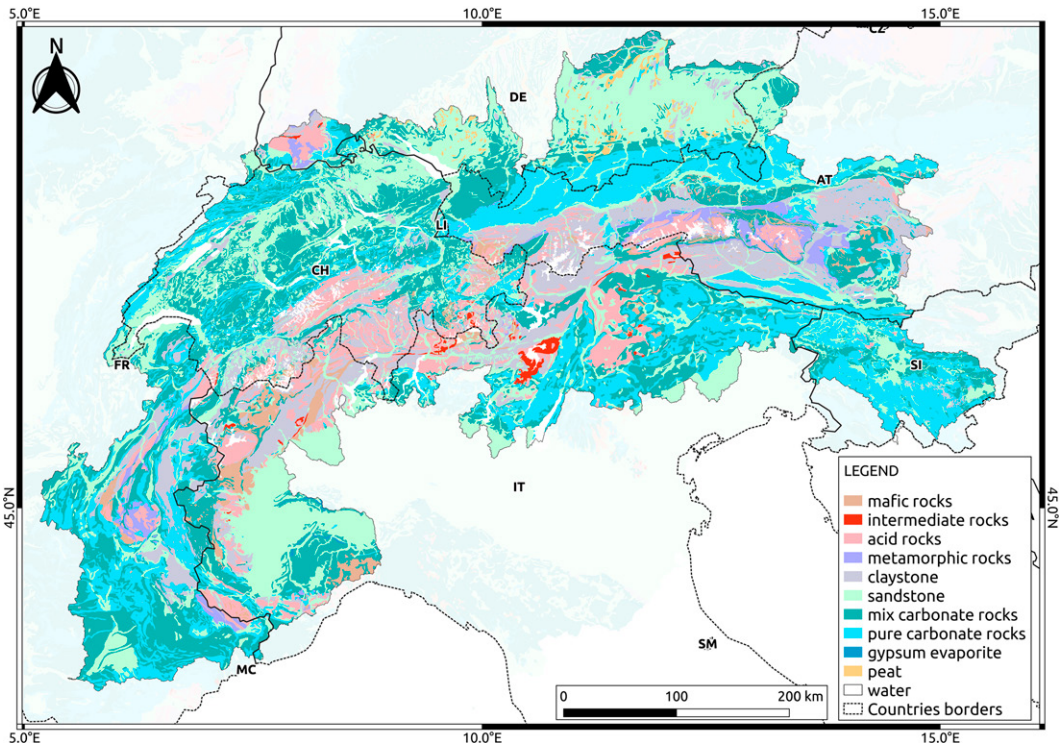

Figure 2. Geo-lithological map of the Alps (Alpine-Geo-LiM), scale: 1:1,000,000. IT—Italy, MC—Monte Carlo, AT—Austria, CH—Switzerland, FR—France, DE—Germany, SI—Slovenia, LI—Liechtenstein, SM—San Marino.

TABLE 1. RELATIVE ABUNDANCE (% AREA), MEAN, AND STANDARD DEVIATION (SD) OF ELEVATION AND SLOPE

Rock type	% area	Elevation (m above sea level)		Slope (°)	
		Mean	SD	Mean	SD
Sandstone	26.99	698	519	8.50	10.27
Mixed carbonate	23.75	1157	656	18.38	11.81
Pure carbonate	20.82	1279	590	22.55	12.88
Claystone	12.87	1664	703	23.95	11.85
Acid rocks	7.38	1774	704	27.06	11.88
Water (lakes and glaciers)	2.69	1662	1301	12.55	14.72
Mafic rocks	2.69	1666	720	25.06	11.60
Metamorphic rocks	1.81	1775	609	25.68	11.69
Peat	0.48	555	89	2.14	2.52
Intermediate rocks	0.43	1993	619	28.32	11.00
Gypsum evaporite	0.08	603	587	11.50	9.00

"gypsum evaporite" represent less than 1% of the study area (respectively 0.48% and 0.08%). A small area (2.69%) is covered by "water" in the form of lakes and glaciers. The data about the abundance of each outcropping rocks type (% Area in Table 1) in the Alpine region are quite similar to the percentages computed by Donnini et al. (2016), which, however, underestimated the percentage of claystone and did not fully differentiate the metamorphic rocks. Looking at the elevation and slope values reported in Table 1, and based on the 25-m-resolution European digital elevation model (EU-DEM; Bashfield and Keim, 2011; https://www.eea.europa.eu/data-and-maps/data/copernicus-land-monitoring-service-eu-dem), we find that "claystone," "acid rocks," "mafic rocks," "metamorphic rocks," and "intermediate rocks" have the highest mean elevation (from 1664 m to 1993 m) and slope values (from 23.95° to 28.32°) associated with relatively low standard deviation values. This is due to the fact that these lithologies compose the crystalline massifs that are the tallest mountains of the Alps (e.g., Monte Bianco, 4808 m.a.s.l.; Monte Rosa, 4634 m.a.s.l.; Dent Blanche, 4357 m.a.s.l.).

High mean elevation values (1662 m) are associated also with "water" (lakes and glaciers), with a high standard deviation (1301 m); moreover, a medium slope value (12.55°), with a relatively high standard deviation (14.72°), is associated with "water." This big variation is related to the fact that the "water" class includes lakes (which usually are located in the valley) and glaciers (which are located at high altitude).

The mean elevation and the mean slope of "pure carbonate rocks" are equal to 1279 m and 22.55°, respectively. This is confirmed by the fact that the highest calcareous mountains of the Alps have quite high elevations (e.g., Ortles, at 3905 m.a.s.l.; Gran Zebrù, at 3857 m.a.s.l.; and Marmolada, at 3343 m.a.s.l., in the southeastern Eoalpine Calcareous Alps; Parseierspitze, at 3036 m.a.s.l., in the Northern Calcareous Alps; and Crêt de la Neige, at 1720 m.a.s.l. in the Jura Mountains). Table 1 shows that "mixed carbonate rocks," mainly composed by impure carbonate rock, calcarenite, and marl, have mean elevation and slope values, respectively, of 1157 m and 18.38°.

Elevation and slope of the rocks classified within the "sandstone" class are relatively low with respect to the other lithologies (respectively 698 m and 8.50°, with associated standard deviation of 519 m. and 10.27°, respectively). This is due to the fact that we included, in this lithology, conglomerates and uncemented sediments produced by the erosion of the massifs.

"Gypsum evaporite" presents low mean elevation (603 m) and slope (11.50°) values, as does "peat" (555 m; 2.14°). This last observation is not surprising, since "peat" is formed in vegetated and flattened wetlands by the degradation of the vegetation (Bracco et al., 2004).

Lithology of Main River Basins

With the aim to quantify the atmospheric CO_2 consumed by chemical weathering using the forward method, the proportions of the outcropping rocks (Table 2) were estimated for each

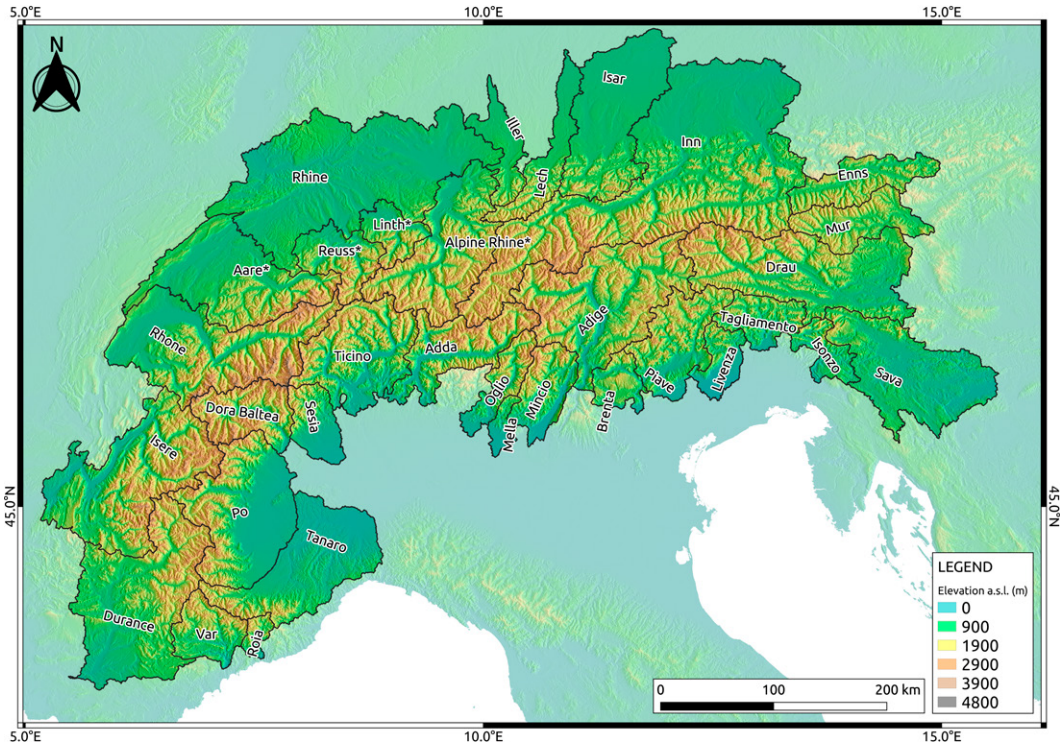

Figure 3. Main Alpine river basins defined by Donnini et al. (2016), including the four Rhine subbasins, highlighted by asterisks.

TABLE 2. PROPORTIONS OF THE LITHOLOGICAL CLASSES FOR EACH RIVER BASIN CALCULATED FROM ALPINE-GEO-LIM

Basin ID	River name	Sandstone (%)	Mixed carbonate (%)	Pure carbonate (%)	Claystone (%)	Acid rocks (%)	Mafic rocks (%)	Metamorphic rocks (%)	Peat (%)	Intermediate rocks (%)	Gypsum evaporite (%)
1	Roia	21.94	40.05	32.28	1.50	3.97	0.00	0.06	0.00	0.00	0.21
2	Mella	50.36	21.97	21.26	5.04	1.27	0.11	0.00	0.00	0.00	0.00
3	Brenta	11.84	27.87	47.74	0.00	11.73	0.82	0.00	0.00	0.00	0.00
4	Isonzo	13.98	28.45	57.37	0.00	0.20	0.00	0.00	0.00	0.00	0.00
5	Livenza	50.81	11.16	38.01	0.02	0.00	0.00	0.00	0.00	0.00	0.00
6	Iller	43.52	38.79	14.03	1.44	0.00	0.00	0.38	1.84	0.00	0.00
7	Oglio	37.23	15.12	14.92	21.75	4.46	0.35	0.00	0.00	6.17	0.00
8	Sesia	44.01	0.74	0.41	25.81	13.22	14.04	0.00	0.00	1.77	0.00
9	Tagliamento	21.36	17.85	59.03	0.35	0.47	0.94	0.00	0.00	0.00	0.00
10	Var	8.60	52.21	23.97	1.28	3.32	0.00	10.62	0.00	0.00	0.00
11	Mincio	16.47	14.00	51.01	3.48	5.74	0.26	0.00	0.00	9.04	0.00
12	Lech	39.67	10.61	46.61	1.55	0.00	0.00	0.01	1.55	0.00	0.00
13	Enns	21.06	13.88	31.79	29.16	3.08	0.84	0.18	0.00	0.00	0.00
14	Mur	9.72	10.74	7.65	51.38	2.88	5.31	12.31	0.00	0.00	0.00
15	Dora Baltea	12.71	21.91	2.42	33.33	7.25	21.32	0.01	0.00	1.04	0.00
16	Piave	21.35	38.62	36.71	0.81	1.51	0.78	0.00	0.00	0.22	0.00
17	Adda	20.61	13.28	7.79	24.30	25.85	4.36	0.97	0.00	2.85	0.01
18	Ticino	17.27	7.59	3.61	32.97	32.94	5.31	0.11	0.00	0.16	0.05
19	Isar	48.46	16.76	24.12	3.83	0.00	0.00	0.00	6.84	0.00	0.00
20	Tanaro	41.65	32.19	5.66	2.63	9.85	6.18	0.51	0.00	0.00	1.32
21	Sava	22.22	18.53	56.43	2.01	0.81	0.00	0.00	0.00	0.00	0.00
22	Po	46.05	17.90	4.51	11.74	9.94	9.64	0.00	0.00	0.09	0.13
23	Adige	13.51	21.69	15.06	22.69	22.59	2.56	0.00	0.00	1.91	0.00
24	Drau	15.39	17.68	20.38	31.54	5.35	3.64	6.02	0.00	0.00	0.00
25	Rhone	31.20	25.02	14.29	17.17	10.04	1.83	0.16	0.00	0.10	0.19
26	Isere	14.76	28.68	25.05	16.77	6.22	2.90	5.62	0.00	0.00	0.00
27	Durance	13.20	40.90	35.08	9.38	0.57	0.06	0.81	0.00	0.00	0.00
28	Inn	31.67	16.34	21.55	14.71	7.62	2.41	4.71	0.78	0.20	0.01
29	Rhine	35.99	34.57	14.92	6.02	5.70	1.23	0.98	0.45	0.09	0.06
30	Linth*	32.01	40.83	16.83	9.70	0.48	0.15	0.00	0.00	0.00	0.00
31	Reuss*	23.36	40.30	15.26	8.73	11.21	1.05	0.00	0.00	0.00	0.09
32	Alpine Rhine*	22.03	35.89	15.27	11.38	9.84	4.76	0.78	0.00	0.02	0.02
33	Aare*	30.78	38.74	22.15	4.18	3.79	0.16	0.00	0.00	0.00	0.21
	mean	*26.81*	*24.57*	*24.34*	*12.32*	*6.72*	*2.76*	*1.34*	*0.35*	*0.72*	*0.07*
	st. dev.	*13.07*	*12.38*	*16.92*	*12.94*	*7.77*	*4.59*	*3.06*	*1.24*	*1.93*	*0.23*

Note: Lakes and glaciers (which represent less than 3% of the total study area) were excluded from the computation.
*Indicates Rhine subbasin.

river basin. We considered all the 33 river basins (Fig. 3) defined in Donnini et al. (2016), including the four Rhine subbasins (Linth, Reuss, Alpine Rhine, and Aare).

Glaciers and lakes pose some uncertainty in estimating atmospheric CO_2 consumption by chemical weathering. Anderson et al. (1997) and Anderson (2005) showed that glaciers increase runoff within basins, but they do not enhance silicate weathering processes. Regarding lakes, Cole et al. (2007) and Tranvik et al. (2009) showed that freshwaters (lakes, rivers, and reservoirs) act both in transporting and in producing the atmospheric carbon (CO_2 and CH_4), confirming the atmospheric CO_2 and CH_4 production in lakes as highlighted by Huttunen et al. (2003), Del Sontro et al. (2010), Diem et al. (2012), and Pighini et al. (2018). In this work, we decided to simplify our approach by considering glaciers and lakes just like parts of the hydrographic network.

In Alpine-Geo-LiM, the sediments of the alluvial valleys and terraces were included in the "sandstone" class. Here, conglomerates and uncemented sediments have been put in place by the erosion, transport, and deposition of the rocks constituting the upper part of the watersheds. As a consequence, one can assume that the lithology of those materials should reflect that of the upstream massifs. It becomes relevant to check if, in the 33 river basins, the sandstones are mainly associated with the presence of carbonate rocks or silicate rocks. To better investigate the association of the "sandstone" class with the other lithologies, we performed a cluster analysis using the well-known unsupervised k-means algorithm (Hartigan and Wong, 1979) implemented in the R software (R Core Team, 2016) and imposing four clusters. The percentages of the lithologies representing the centers of the four clusters are shown in Table 3.

Cluster 1 shows a percentage of "sandstone" equal to 19.72% associated with: (1) 73.80% of carbonate rocks ("mixed carbonate" and "pure carbonate"), (2) 6.24% of "claystone" and igneous and metamorphic rocks ("acid rocks," "mafic rocks," "metamorphic rocks," and "intermediate rocks"), and (3) 0.26% of other lithologies ("peat" and "gypsum evaporite").

Cluster 2 shows a similar percentage of "sandstone" (15.02%) associated with a relatively low percentage of carbonate rocks (28.66%), and a high percentage of "claystone" and igneous and metamorphic rocks (56.32%). Other lithologies ("peat" and "gypsum evaporite") are negligible (0.01%).

In cluster 3, the "sandstone" percentage is equal to 20.74%, carbonate rocks are 64.46%, "claystone" and igneous and metamorphic rocks are 14.75%, and other rocks are 0.06%.

Cluster 4 shows relatively high concentration of "sandstone" (40.79%), followed by carbonate rocks (37.86%) and by "claystone" and igneous and metamorphic rocks (20.29%). As for the other clusters, other lithologies have a low percentage (1.06%).

The analysis shows that the "sandstone" class is associated with a high percentage of "claystone" and igneous and metamorphic rocks only in cluster 2, while in the other

TABLE 3. RESULT OF THE CLUSTER ANALYSIS

Cluster	Sandstone (%)	Mixed carbonate (%)	Pure carbonate (%)	Claystone (%)	Acid rocks (%)	Mafic rocks (%)	Metamorphic rocks (%)	Peat (%)	Intermediate rocks (%)	Gypsum evaporite (%)
1	19.72	20.68	53.12	1.23	3.16	0.34	0	0.26	1.51	0
2	15.02	15.98	12.68	30.85	14.28	6.19	4.15	0	0.85	0.01
3	20.74	39.73	24.73	7.08	4.56	1.1	1.98	0	0.03	0.06
4	40.79	22.1	15.76	9.02	5.65	3.25	1.6	0.9	0.77	0.16

clusters (including cluster 4 characterized by high "sandstone" concentration), "sandstone" is associated with a high percentage of carbonate rocks. Since the "sandstone" lithology is produced by the erosion of the massifs, we maintain that in the studied area, "sandstone" is mostly composed of carbonate rocks.

Figure 4 shows the spatial distribution of the four clusters, highlighting (1) the presence of an inner core mainly composed of crystalline silicate rocks (mainly "claystone"; cluster 2), (2) a western and eastern (mainly) bound with carbonate rocks (cluster 1 and cluster 3), and (3) "sandstone" rocks (cluster 4) in the northern and southern sectors of the Alps (Molasse Basin and Po Valley) composed of sandstone rich in carbonates (see Appendix A [text footnote 1]).

RELATIONSHIPS AMONG LITHOLOGY, RIVER ALKALINITY, AND ATMOSPHERIC CO_2 CONSUMPTION

Input Data

To estimate the atmospheric CO_2 consumed by chemical weathering in the Alpine region, we applied a revised version of the forward method (Hartmann, 2009; Hartmann et al., 2009).

For the purpose, we considered the subdivision of the Alpine region in 33 river basins (Fig. 3) from Donnini et al. (2016) and the alkalinity of river waters sampled near the basin outlets during spring and winter seasons in the 2011–2012 hydrological year (Donnini et al., 2016).

Table 4 shows the data on alkalinity and flow rate for the 33 sampled river basins in Donnini et al. (2016). In the table, the suffixes (s) and (w) refer to the two sampling campaigns (s: spring season, w: winter season). $[HCO_3]_{(s)}$ and $[HCO_3]_{(w)}$ represent the alkalinity of river waters sampled in the two sampling campaigns; $Q_{(s)}$ and $Q_{(w)}$ represent the daily discharge at the time of the two sampling campaigns; and $Q_{(my)}$ represents the mean annual discharge expressed in m^3/s estimated by using the daily discharge measured in one hydrological year. $PD[HCO_3]_{(w/s)}$ and $PD[Q]_{(w/s)}$ are the percentage difference respectively calculated between $[HCO_3]_{(w)}$ and $[HCO_3]_{(s)}$, and between $Q_{(w)}$ and $Q_{(s)}$ by using the following equation:

$$PD[X]_{(w/s)} = ([X]_{(w)} / [X]_{(s)} \times 100 - 100)\%. \quad (10)$$

The data on discharges were obtained from different sources, including international, national, and local authorities (see references in Table 4). For most catchments, the data were available as flow rates (m^3/s); for the catchments where only stage measurements (m) at gauging stations were available, the stage measurements were converted to estimated discharge (m^3/s) by using rating curves provided by river basin authorities or derived using empirical data.

Table 4 shows that data on flow rate markedly varied within the two sampling campaigns, with mean $PD[Q]_{(w/s)}$ of 3.06%, and a coefficient of variation equal to 23.79%. Moreover, Table 4 shows that 22 rivers (almost 70% of considered rivers) have the lowest flows in winter season and the highest in spring season ($PD[Q]_{(w/s)} > 0$), which is typical of rivers with glacial- and snowmelt-dominated regimes. A comparison of $Q_{(s)}$ and $Q_{(w)}$ with $Q_{(my)}$ highlights the fact that almost all the flow rate values, measured at the time of the two sampling campaign, were lower than the mean annual discharge estimated considering the daily discharge in one hydrological year. On the contrary, Table 4 shows that alkalinity values are less variant across the seasonal measurements with respect to the flow rates, having mean $PD[HCO_3]_{(s/w)}$ of 17.38% and a variation coefficient equal to 1.40%. More generally, it seems that there is not a correlation between the flow rate and the alkalinity. The weak correlation between flow rate and alkalinity is also shown in Figure 5, where the alkalinity (HCO_3) of the river waters sampled in the two campaigns (in spring season and in winter season) is plotted with respect to the

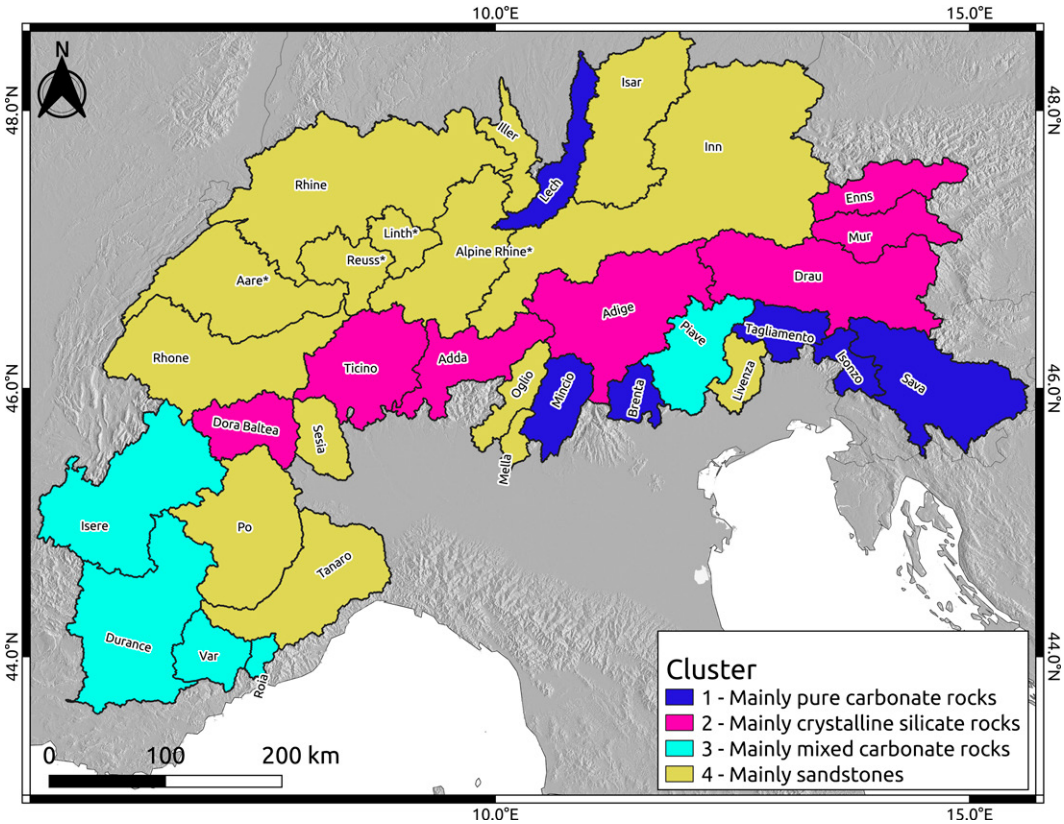

Figure 4. Result of the cluster analysis performed by using R software (R Core Team, 2016).

TABLE 4. DATA ON THE 33 SAMPLED RIVER BASINS

Basin ID	River name	$[HCO_3]_{(s)}$ (mol/L)	$[HCO_3]_{(w)}$ (mol/L)	$Q_{(s)}$ (m^3/s)	$Q_{(w)}$ (m^3/s)	$Q_{(my)}$ (m^3/s)	$PD(HCO_3)_{(s/w)}$ (%)	$PD(Q)_{(s/w)}$ (%)	Ref.
1	Roia	1.66×10^{-3}	2.56×10^{-3}	6.67	3.38	11.93	54.22	–49.33	1
2	Mella	4.95×10^{-3}	4.79×10^{-3}	3.35	7.80	16.74	–3.27	132.84	2
3	Brenta	2.03×10^{-3}	2.67×10^{-3}	44.70	42.30	61.77	31.42	–5.37	3
4	Isonzo	2.63×10^{-3}	2.80×10^{-3}	42.00	73.10	161.75	6.22	74.05	4
5	Livenza	3.08×10^{-3}	2.88×10^{-3}	76.30	32.40	42.12	–6.57	–57.54	3
6	Iller	3.16×10^{-3}	4.06×10^{-3}	17.93	36.50	42.40	28.26	103.57	5
7	Oglio	1.95×10^{-3}	1.66×10^{-3}	27.49	46.05	54.91	–14.95	67.52	6
8	Sesia	1.41×10^{-3}	1.85×10^{-3}	43.51	7.30	73.89	31.84	–83.22	7
9	Tagliamento	1.79×10^{-3}	2.50×10^{-3}	20.51	73.72	77.57	39.45	259.43	4
10	Var	1.42×10^{-3}	2.54×10^{-3}	29.10	20.10	37.31	79.03	–30.93	1
11	Mincio	2.37×10^{-3}	1.91×10^{-3}	5.19	4.89	7.83	–19.47	–5.78	8
12	Lech	3.27×10^{-3}	3.60×10^{-3}	63.20	112.00	99.96	10.19	77.22	5
13	Enns	1.84×10^{-3}	2.38×10^{-3}	81.96	36.88	72.49	29.90	–55.00	9
14	Mur	1.54×10^{-3}	2.47×10^{-3}	44.10	25.80	49.52	60.35	–41.50	9
15	Dora Baltea	1.47×10^{-3}	1.69×10^{-3}	64.60	42.30	78.83	15.16	–34.52	7
16	Piave	2.79×10^{-3}	3.36×10^{-3}	42.44	25.96	61.99	20.23	–38.83	3
17	Adda	1.37×10^{-3}	1.27×10^{-3}	110.80	145.60	168.96	–7.39	31.41	10
18	Ticino	8.46×10^{-3}	6.75×10^{-3}	248.00	185.00	178.88	–20.21	–25.40	11
19	Isar	4.48×10^{-3}	4.62×10^{-3}	46.80	32.50	49.43	3.32	–30.56	5
20	Tanaro	2.83×10^{-3}	3.31×10^{-3}	121.00	61.00	137.39	16.67	–49.59	7
21	Sava	3.21×10^{-3}	3.37×10^{-3}	105.74	95.03	269.21	4.97	–10.13	12
22	Po	1.90×10^{-3}	1.88×10^{-3}	80.30	58.90	150.81	–0.83	–26.65	7
23	Adige	1.76×10^{-3}	1.87×10^{-3}	158.77	102.68	216.51	6.39	–35.33	8
24	Drau	2.02×10^{-3}	2.28×10^{-3}	110.17	66.38	256.87	12.95	–39.75	9
25	Rhone	1.57×10^{-3}	1.81×10^{-3}	233.00	333.00	232.28	15.88	42.92	1
26	Isere	1.80×10^{-3}	2.67×10^{-3}	377.06	212.95	238.94	48.36	–43.52	1
27	Durance	2.25×10^{-3}	3.29×10^{-3}	9.26	8.20	18.20	46.23	–11.45	1
28	Inn	2.78×10^{-3}	2.83×10^{-3}	450.21	218.73	561.79	1.52	–51.42	9
29	Rhine	2.43×10^{-3}	2.77×10^{-3}	564.00	708.00	837.70	14.15	25.53	13
30	Linth*		2.43×10^{-3}		61.18	61.73			14
31	Reuss*		1.81×10^{-3}		53.40	105.78			13
32	Alpine Rhine*		2.99×10^{-3}		9.51	240.79			13
33	Aare*		2.70×10^{-3}		175.77	131.66			13

Note: The suffix *(s)* means "spring season" and *(w)* means "winter season." $[HCO_3]_{(s)}$ and $[HCO_3]_{(w)}$ are the river water alkalinity values. $Q_{(s)}$ and $Q_{(w)}$ are the daily discharge at the time of the sampling campaign. $Q_{(my)}$ is the mean annual discharge. $PD[HCO_3]_{(s/w)}$ and $PD[Q]_{(s/w)}$ are the percentage difference respectively calculated between $[HCO_3]_{(s)}$ and $[HCO_3]_{(w)}$, and between $Q_{(s)}$ and $Q_{(w)}$. References: 1: geoportal of the French Ministry of Ecology, Sustainable Development and Energy (www.hydro.eaufrance.fr); 2: ARPA Lombardia (2012); 3: ARPA Veneto (2012); 4: Friuli-Venezia Giulia Region (2012); 5: geoportal of the Environmental Agency of Bavaria (www.hnd.bayern.de); 6: geoportal of the Consorzio dell'Oglio (www.oglioconsorzio.it); 7: ARPA Piemonte (2012); 8: Ufficio Dighe Servizio Prevenzione Rischi Protezione Civile Provincia Autonoma di Trento (2012); 9: geoportal of the Federal Ministry of Sustainability and Tourism of Austria (eHYD) (https://www.ehyd.gv.at/); 10: Consorzio dell'Adda (2012); 11: geoportal of the Consorzio del Ticino (www.ticinoconsorzio.it); 12: Meteorological and Hydrological Service of Croatia (2012); 13: International Commission for the Hydrology of the Rhine basin (CHR/KHR) (2012); 14: Federal Geoportal of Switzerland (https://www.hydrodaten.admin.ch/en).
*Indicates Rhine subbasins that were sampled only in winter season.

flow rate (Q) of the river waters registered at the moment of the two sampling campaigns.

Correlation between Lithology and Water Alkalinity

Starting from the alkalinity of the 33 river waters (sampled in spring and in winter seasons) and from the lithological composition of the 33 rivers basins (computed using Alpine-Geo-LiM), we applied an approach derived from Hartmann et al. (2009) to investigate the relationship between alkalinity and lithology. We performed a multilithological regression using the following linear equation:

$$[HCO_3] = \sum_{i=1}^{n} (SR_i \times b_i). \quad (11)$$

where $[HCO_3]$ is the alkalinity expressed in mol L^{-1}, SR_i is the proportion (from 0 to 1) of the surface area covered by the lithology i derived from Alpine-Geo-LiM, and b_i is a coefficient estimated for each lithology i and obtained by linear multiple regression analysis.

We performed the analysis considering the 10 lithological classes of Table 2, and, due to the scarce presence of some lithologies in the study area, also considering four general lithological classes defined according to the following schema: (1) "sandstone," (2) "claystone," (3) "total carbonate" (including "pure carbonate," "mixed carbonate," "gypsum evaporite," and "peat"), and (4) "igneous and metamorphic rocks" (including "acid rocks," "mafic rocks," "intermediate rocks," and "metamorphic rocks").

Analysis Performed with 10 Lithological Classes

The coefficients resulting from the linear multiple regression analysis performed considering 10 lithological classes are shown in Table 5, where b represents the estimated coefficient for each lithology; *Std Error* measures the standard error in b estimation; the *P value* expresses the probability that the b value is equal to 0 by chance; and *Significance level* is a literal classification of the *P value* expressing the reliability of the analysis.

High b values are correlated with relevant HCO_3^- concentrations and therefore identify lithologies more prone to consuming atmospheric CO_2 by chemical weathering. Conversely, a low value of b is indicative of a low atmospheric CO_2 consumption by chemical weathering from the corresponding lithology. Small *P values* indicate weak correlations between the predictor ($[HCO_3]$) and response (SR) variables. High *P values* correspond to low significance (*Significance level* in Table 5) of the analysis.

Figure 6 shows the alkalinity values of the Alpine rivers measured during the two sampling campaigns (Alkalinity observed) versus the alkalinity values of the same Alpine rivers predicted by applying Equation 11 (Alkalinity predicted). The coefficient of determination (R^2) of the linear fit (passing through the zero) between measured and fitted values is close to 1 (0.95), while the median, the mean, and the standard deviation of the residuals are -3.742×10^{-5}, -1.92×10^{-9}, and 5.335×10^{-4} respectively, highlighting the capability of the model in reproducing the observed data.

In Table 5, the lithologies are ordered from the highest to the lowest b value. The table shows very high chemical alterability and related CO_2 consumption rates for "gypsum evaporites" and "peat" (high b values, respectively, equal to 2.35×10^{-2} mol L^{-1} and 2.2×10^{-2} mol L^{-1}), with very low significance for "gypsum evaporites" (*P value* = 0.51) and high significance for "peat" (*P value* = 0.0017).

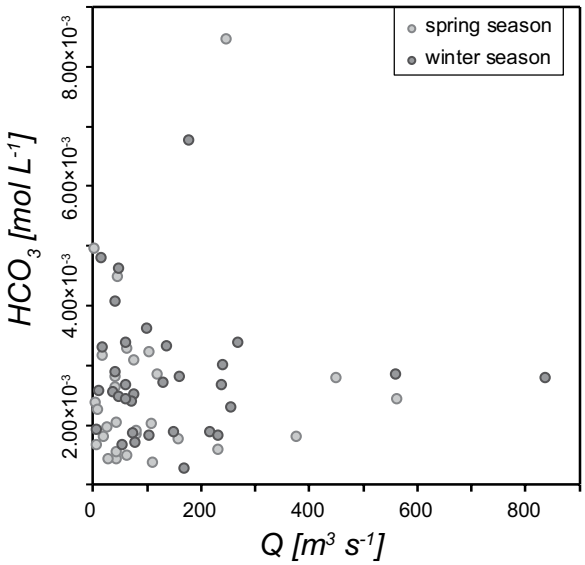

Figure 5. Plot showing the alkalinity (HCO_3) of the river waters sampled in the two campaigns (in spring season and in winter season) vs. the flow rate (*Q*) of the river waters registered at the moment of the two sampling campaigns.

TABLE 5. RESULTS OF THE LINEAR MULTIPLE (*lm*) REGRESSION ANALYSIS

Lithology	*b* (mol L^{-1})	*Std Error*	*P value*	*Significance level*
Gypsum evaporites	2.35×10^{-2}	3.58×10^{-2}	0.51	Very low
Peat	2.2×10^{-2}	6.66×10^{-3}	0.0017	High
Sandstone	4.13×10^{-3}	5.22×10^{-4}	1.77×10^{-10}	Very high
Pure carbonate	2.62×10^{-3}	4.37×10^{-4}	2.03×10^{-7}	Very high
Mixed carbonate	2.32×10^{-3}	5.79×10^{-4}	1.96×10^{-4}	Very high
Metamorphic rocks	2.28×10^{-3}	3.19×10^{-3}	0.48	Very low
Claystone	1.44×10^{-3}	9.01×10^{-4}	0.12	Low
Mafic rocks	-2.37×10^{-4}	2.10×10^{-3}	0.91	Very low
Acid rocks	-1.64×10^{-3}	1.15×10^{-3}	0.16	Very low
Intermediate rocks	-3.98×10^{-3}	4.00×10^{-3}	0.32	Very low

Note: *b* value represents the calibration parameter estimated for each lithology, *Std Error* measures the standard error in *b* estimation, *P value* expresses the probability that the coefficient is equal to 0 by chance. *Significance level* codes: very high (*P value* < 0–0.001), high (*P value* = 0.001–0.01), medium (*P value* = 0.01–0.05), low (*P value* = 0.05–0.1), very low (*P value* = 0.1–1).

High *b* values are shown for "sandstone" ($b = 4.13 \times 10^{-3}$ mol L^{-1}), with very high significance (*P value* = 1.77×10^{-10}), and "pure carbonate" and "mixed carbonate" (*b* values, respectively, equal to 2.62×10^{-3} mol L^{-1} and 2.32×10^{-3} mol L^{-1}; *P values* = 2.03×10^{-7} and 1.96×10^{-4}, respectively).

Very low *b* values together with low significance are shown for "metamorphic rocks" ($b = 2.28 \times 10^{-3}$ mol L^{-1}; *P value* = 0.48) and "claystone" ($b = 1.44 \times 10^{-3}$ mol L^{-1}; *P value* = 0.12).

Negative *b* values were obtained for "mafic rocks," "acid rocks," and "intermediate rocks," associated with very low significance and *P values*.

These results show a surprising behavior of "peat," with a positive and highly significant value of the calibration parameter *b*. Since peat is composed by at least 30% of organic matter (Joosten and Clarke, 2002), its dissolution leads to the release of organic carbon into the atmosphere (e.g., Chow et al., 2003; Bengtsson and Törneman, 2004; Schwalm and Zeitz, 2015; Selvam et al., 2017); for this reason, we would have expected a negative value of *b*. This discrepancy could be explained by the fact that the "peat" presence is concentrated in the Isar basin (6.84% of the basin), where it is associated with "sandstone" (41.6%), "pure carbonate" (24.12%), and "mixed carbonate" (16.76%), i.e., lithologies particularly effective at CO_2 consumption.

The relative high values of the *Std Error* values (and low *P values*) obtained for "mafic rocks," "acid rocks," and "intermediate rocks" demonstrate that the values of the *b* coefficients are not statistically different from 0, and therefore that the contribution of these lithologies to the CO_2 consumption is negligible.

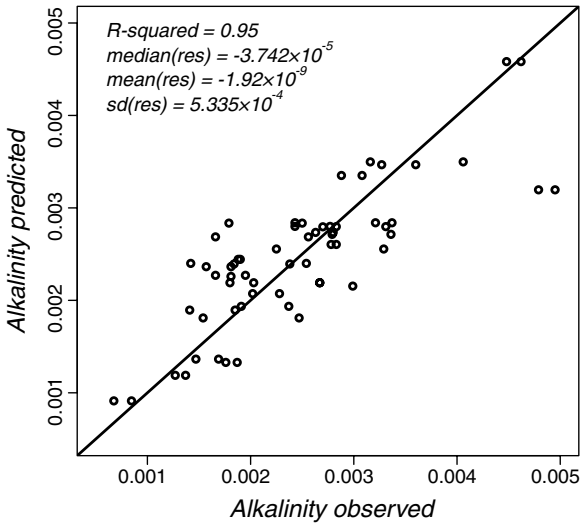

Figure 6. Plot showing the alkalinity values of the Alpine rivers measured during the two sampling campaigns (*Alkalinity observed*) vs. the alkalinity values of the same Alpine rivers predicted by applying linear multiple (*lm*) regression analysis (*Alkalinity predicted*). *R-squared* is the coefficient of determination of the linear fit passing through zero (R^2); *median(res)*, *mean(res)*, and *sd(res)* are, respectively, the median, the mean, and the standard deviation of the residuals.

Analysis Performed with Four Lithological Classes

Two other linear multiple regression analyses were performed using the linear multiple (*lm*) and the multiple nonnegative linear (*nnl*) regression analysis tools in the R software (R Core Team, 2016) considering the following four lithological classes: (1) "sandstone," (2) "claystone," (3) "total carbonate" (including "pure carbonate," "mixed carbonate," "gypsum evaporite," and "peat"), and (4) "igneous and metamorphic rocks" (including "acid rocks," "mafic rocks," "intermediate rocks," and "metamorphic rocks"). Table 6 shows the values of the *b* coefficients obtained by modeling the lithologies with the *lm* and *nnl* regression models (R Core Team, 2016). We observe that in the *lm* model, all the coefficients are significant (very high significance for "sandstone" and "total carbonate," and medium significance for "claystone" and "igneous and metamorphic rocks"). Moreover, we note that the *b* value for the "igneous and metamorphic rocks" is still negative. This value does not agree with the assumptions that acid, mafic, intermediate, and metamorphic rocks are involved in a process of CO_2 consumption (Eqs. 1–4). For this reason, in Table 6, we also show the values of the *b* coefficients obtained using a nonnegative linear (*nnl*) regression analysis. We observe that, as expected, the *b* value for "igneous and metamorphic rocks" becomes 0, whereas the coefficients of "sandstone" and "total carbonate" do not significantly change with respect to the values obtained with the

TABLE 6. RESULTS OF THE LINEAR MULTIPLE (*lm*) AND NONNEGATIVE (*nnl*) REGRESSION ANALYSES

	lm regression analysis				*nnl* regression analysis
	b (mol L^{-1})	*Std Error*	*P value*	*Significance level*	*b* (mol L^{-1})
Sandstone	4.65×10^{-3}	4.39×10^{-4}	3.42×10^{-15}	Very high	4.50×10^{-3}
Claystone	2.00×10^{-3}	7.87×10^{-4}	0.0138	Medium	6.30×10^{-4}
Total carbonate	2.48×10^{-3}	2.28×10^{-4}	1.16×10^{-15}	Very high	2.45×10^{-3}
Igneous and metamorphic rocks	-2.08×10^{-3}	9.24×10^{-4}	0.0284	Medium	0

Note: *b* value represents the calibration parameter estimated for each lithology, *Std Error* measures the standard error in *b* estimation, *P value* expresses the probability that the coefficient is equal to 0 by chance. *Significance level* codes: very high (*P value* < 0–0.001), high (*P value* = 0.001–0.01), medium (*P value* = 0.01–0.05), low (*P value* = 0.05–0.1), very low (*P value* = 0.1–1).

lm regression. Conversely, the *b* coefficient of "claystone" obtained using the *nnl* model (6.30×10^{-4} mol L^{-1}) is lower with respect to the values obtained using the *lm* regression (2.00×10^{-3} mol L^{-1}). The determination coefficient of the fitting between the measured concentrations and the fitted values of the *lm* regression (R^2) is again equal to 0.95, whereas the median, the mean, and the standard deviation of the residuals are -5.035×10^{-5}, -1.65×10^{-9}, and 5.935×10^{-4} respectively. Analogue values for the *nnl* model were obtained (R^2: 0.94, residuals median: 5.943×10^{-5}, residuals mean: 1.453×10^{-5}, residuals standard deviation: 6.187×10^{-4}).

The linear model derived using four lithological classes was tested against a model built using literature values and in particular the *b* values estimated by Amiotte Suchet et al. (2003). In particular, we assumed *b* equal to (1) 1.52×10^{-4} for "sandstone," (2) 6.27×10^{-4} for "claystone," (3) 3.17×10^{-3} for "total carbonate" and (4) 9.50×10^{-5} for "igneous and metamorphic rocks." Residuals between the linear model built using the Amiotte Suchet et al. (2003) coefficients and the measured alkalinity have values of median, mean, and the standard deviation respectively equal to -6.74×10^{-4}, -7.86×10^{-4}, and 9.06×10^{-4}. As expected, the model built using the Amiotte Suchet et al. (2003) coefficients is less accurate (larger absolute values of mean and median values) and precise (larger standard deviation) in predicting the original alkalinity values with respect to the proposed model derived using four lithological classes.

Amount of Atmospheric CO_2 Fixed by Chemical Weathering

The flux of atmospheric CO_2 consumed by chemical weathering on the "short-term," namely $\phi(CO2)_{short}$, was estimated considering the following equation derived from Hartmann et al. (2009):

$$\phi(CO_2)_{short} = RO \times \Sigma_{i=1}^{n}(SR_i \times b_i \times a), \quad (12)$$

where *RO* is the runoff, SR_i is the proportion (from 0 to 1) of the surface area covered by lithology *i*, b_i is the calibration parameter for lithology *i*, and *a* is a parameter having value 1 in case of silicate rocks and value 0.5 in case of carbonate rocks (see Eq. 9).

Table 7 shows the fluxes, $\phi(CO_2)_{short}$, of atmospheric CO_2 consumed by chemical weathering and estimated at basin scale by applying Equation 12. The values of *b* coefficients were derived by the *lm* regression analysis performed using 10 lithologies (see Table 5). Where the *Significance level* of the *b* values was very low (i.e., for "gypsum evaporites," "metamorphic

TABLE 7. FLUXES OF ATMOSPHERIC CO_2 CONSUMED BY CHEMICAL WEATHERING, $\Phi(CO_2)_{short}$, WITHIN THE MAIN ALPINE RIVER BASINS ESTIMATED CONSIDERING "SANDSTONE" COMPOSED MAINLY BY SILICATE ROCKS (SILICATE-SANDSTONE SCENARIO) AND MAINLY BY CARBONATE ROCKS (CARBONATE-SANDSTONE SCENARIO)

Basin ID	River name	Silicate-sandstone scenario			Carbonate-sandstone scenario			$PD[\Phi(CO_2)_{S(my)}]_{(carb/sil)}$
		$\Phi(CO_2)_{S(s)}$ (mol km^{-2} yr^{-1})	$\Phi(CO_2)_{S(w)}$ (mol km^{-2} yr^{-1})	$\Phi(CO_2)_{S(my)}$ (mol km^{-2} yr^{-1})	$\Phi(CO_2)_{S(s)}$ (mol km^{-2} yr^{-1})	$\Phi(CO_2)_{S(w)}$ (mol km^{-2} yr^{-1})	$\Phi(CO_2)_{S(my)}$ (mol km^{-2} yr^{-1})	(%)
1	Roia	5.76×10^5	2.92×10^5	1.03×10^6	4.32×10^5	2.19×10^5	7.73×10^5	–24.96
2	Mella	3.70×10^5	8.61×10^5	1.85×10^6	2.27×10^5	5.28×10^5	1.13×10^6	–38.72
3	Brenta	1.27×10^6	1.20×10^6	1.75×10^6	1.05×10^6	9.94×10^5	1.45×10^6	–17.01
4	Isonzo	1.36×10^6	2.38×10^6	5.26×10^6	1.13×10^6	1.96×10^6	4.34×10^6	–17.40
5	Livenza	3.71×10^6	1.57×10^6	2.05×10^6	2.28×10^6	9.68×10^5	1.26×10^6	–38.49
6	Iller	7.85×10^5	1.60×10^6	1.86×10^6	5.38×10^5	1.09×10^6	1.27×10^6	–31.47
7	Oglio	9.17×10^5	1.54×10^6	1.83×10^6	6.00×10^5	1.00×10^6	1.20×10^6	–34.61
8	Sesia	1.32×10^6	2.21×10^5	2.23×10^6	7.73×10^5	1.30×10^5	1.31×10^6	–41.25
9	Tagliamento	5.23×10^5	1.88×10^6	1.98×10^6	4.00×10^5	1.44×10^6	1.51×10^6	–23.62
10	Var	4.25×10^5	2.93×10^5	5.45×10^5	3.66×10^5	2.53×10^5	4.70×10^5	–13.74
11	Mincio	8.79×10^4	8.29×10^4	1.33×10^5	6.88×10^4	6.48×10^4	1.04×10^5	–21.79
12	Lech	1.88×10^6	3.33×10^6	2.97×10^6	1.31×10^6	2.33×10^6	2.08×10^6	–29.94
13	Enns	5.88×10^5	6.83×10^5	1.34×10^6	1.16×10^6	5.24×10^5	1.03×10^6	–23.29
14	Mur	1.75×10^6	3.44×10^5	6.60×10^5	5.02×10^5	2.94×10^5	5.63×10^5	–14.69
15	Dora Baltea	7.38×10^5	4.83×10^5	9.00×10^5	5.88×10^5	3.85×10^5	7.17×10^5	–20.34
16	Piave	5.30×10^5	3.24×10^5	7.75×10^5	4.02×10^5	2.46×10^5	5.87×10^5	–24.19
17	Adda	1.08×10^6	1.42×10^6	1.65×10^6	7.66×10^5	1.01×10^6	1.17×10^6	–29.21
18	Ticino	1.56×10^6	1.17×10^6	1.13×10^6	1.14×10^6	8.52×10^5	8.24×10^5	–26.95
19	Isar	7.70×10^5	5.35×10^5	8.13×10^5	5.81×10^5	4.03×10^5	6.14×10^5	–24.58
20	Tanaro	1.03×10^6	5.19×10^5	1.17×10^6	6.28×10^5	3.16×10^5	7.13×10^5	–39.00
21	Sava	7.60×10^5	6.83×10^5	1.94×10^6	5.77×10^5	5.18×10^5	1.47×10^6	–24.14
22	Po	6.54×10^5	4.79×10^5	1.23×10^6	3.88×10^5	2.84×10^5	7.28×10^5	–40.68
23	Adige	6.55×10^5	4.24×10^5	8.94×10^5	5.18×10^5	3.35×10^5	7.07×10^5	–20.92
24	Drau	5.20×10^5	3.14×10^5	1.21×10^6	4.14×10^5	2.50×10^5	9.66×10^5	–20.35
25	Rhone	1.41×10^6	2.01×10^6	1.41×10^6	9.62×10^5	1.38×10^6	9.59×10^5	–32.00
26	Isere	1.61×10^6	9.09×10^6	1.02×10^6	1.28×10^6	7.26×10^5	8.14×10^5	–20.16
27	Durance	3.93×10^4	3.48×16^4	7.73×10^4	3.27×10^4	2.89×10^4	6.42×10^4	–16.89
28	Inn	1.29×10^6	6.27×10^5	1.61×10^6	9.00×10^5	4.37×10^5	1.12×10^6	–30.24
29	Rhine	1.10×10^6	1.38×10^6	1.63×10^6	7.38×10^5	9.27×10^5	1.10×10^6	–32.76
30	Linth*		2.92×10^6	2.31×10^6		1.59×10^6	1.60×10^6	–30.66
31	Reuss*		1.04×10^6	2.07×10^6		7.57×10^5	1.50×10^6	–27.44
32	Alpine Rhine*		6.58×10^4	1.67×10^6		4.81×10^4	1.22×10^6	–26.92
33	Aare*		1.39×10^6	1.04×10^6		9.61×10^5	7.20×10^5	–30.69
	Mean	*1.00×10^6*	*9.81×10^5*	*1.52×10^6*	*7.16×10^5*	*7.05×10^5*	*1.09×10^6*	*–26.94*

Note: The fluxes were estimated considering three values of runoff calculated from $Q_{(s)}$, $Q_{(w)}$, and $Q_{(my)}$ (see Table 4). $PD[\Phi(CO_2)_{S(my)}]_{carb/sil)}$ represents the percentage difference between the mean annual fluxes, $\Phi(CO_2)_{S(my)}$, estimated considering the carbonate-sandstone scenario and the silicate-weathering scenario.
*Indicates Rhine subbasins that were sampled only in winter season.

rocks," "mafic rocks," "acid rocks," and "intermediate rocks," as shown in Table 5), we considered *b* equal to 0. This choice is reinforced by the fact that (1) if the *Significance level* of *b* is very low, it means that *b* is statistically not different from 0, and (2) the negative *b* values for "mafic rocks," "acid rocks," and "intermediate rocks" do not agree with the assumption that these lithologies are involved in the CO_2 consumption processes (see Eqs. 1–4). The CO_2 fluxes were then calculated considering that "sandstone" is composed mainly either by silicate rocks (silicate-sandstone scenario) or by carbonate rocks (carbonate-sandstone scenario). In the silicate-sandstone scenario, the *a* parameter was considered equal to 0.5 only for pure carbonate and mixed carbonate categories and 1 for the remaining rock categories. In the carbonate-sandstone scenario, the *a* parameter was considered equal to 0.5 for pure carbonate, mixed carbonate, and sandstone categories and 1 for the remaining rock categories. Finally, *RO* values were calculated from $Q_{(s)}$, $Q_{(w)}$, and $Q_{(my)}$ (see Table 4), leading to three sets of $\phi(CO_2)_{short}$ for each scenario: $\phi(CO_2)_{S(s)}$, $\phi(CO_2)_{S(w)}$, and $\phi(CO_2)_{S(my)}$.

Considering the silicate-sandstone scenario, Table 7 shows that during the spring season, the flux of atmospheric CO_2 consumed by chemical weathering, $\phi(CO_2)_{S(s)}$, ranges from 3.93×10^4 mol km^{-2} yr^{-2} (Durance) to 3.71×10^6 mol km^{-2} y^{-2} (Livenza). Similar values were obtained by using both $Q_{(w)}$ and $Q_{(my)}$, since: (1) $\phi(CO_2)_{S(w)}$ ranges from 3.48×10^4 mol km^{-2} yr^{-2} (Durance) to 3.33×10^6 mol km^{-2} yr^{-2} (Lech), and (2) $\phi(CO_2)_{S(my)}$ ranges from 7.73×10^4 mol km^{-2} yr^{-2} (Durance) to 5.26×10^6 mol km^{-2} yr^{-2} (Isonzo). Also, the average values of $\phi(CO_2)_{S(s)}$, $\phi(CO_2)_{S(w)}$, and $\phi(CO_2)_{S(my)}$ were quite similar, being 9.43×10^5 mol km^{-2} yr^{-2}, 9.81×10^5 mol km^{-2} yr^{-2}, and 1.52×10^6 mol km^{-2} yr^{-2}, respectively.

The lowest $\phi(CO_2)_{short}$ values were systematically obtained considering the carbonate-sandstone scenario, since the *a* parameter for "sandstone" for this scenario was considered equal to 0.5, in contrast to the carbonate-sandstone scenario, where the *a* parameter was considered equal to 1. Considering the spring season, $\phi(CO_2)_{S(s)}$ ranged from 3.27×10^4 mol km^{-2} yr^{-2} (Durance) to 2.28×10^6 mol km^{-2} yr^{-2} (Livenza); considering the winter season, $\phi(CO_2)_{S(w)}$ varied from 2.89×10^4 mol km^{-2} yr^{-2} (Durance) to 2.33×10^6 mol km^{-2} yr^{-2} (Lech); and considering $Q_{(my)}$, the $\phi(CO_2)_{S(my)}$ ranged from 6.24×10^4 mol km^{-2} yr^{-2} (Durance) to 4.34×10^6 mol km^{-2} yr^{-2} (Isonzo). Quite similar values were obtained considering the average values of $\phi(CO_2)_{S(s)}$, $\phi(CO_2)_{S(w)}$, and $\phi(CO_2)_{S(my)}$, which were, respectively, 6.89×10^5 mol km^{-2} yr^{-2}, 7.05×10^5 mol km^{-2} yr^{-2}, and 1.09×10^6 mol km^{-2} yr^{-2}.

In Table 7, $PD[\phi(CO_2)_{S(my)}]_{(carb/sil)}$ represents the percentage difference, calculated following Equation 10, between the two values of $\phi(CO_2)_{S(my)}$ computed considering the carbonate-sandstone scenario and the silicate-sandstone scenario. The obtained percentage differences show that in the carbonate-sandstone scenario, the $\phi(CO_2)_{S(my)}$ value is on average –26.94% with respect to the fluxes estimated in the silicate-sandstone scenario, with the minimum value of –41.25% for Sesia and the maximum value of –13.74% for Var.

The fluxes of atmospheric CO_2 consumed by chemical weathering coming from silicates, $\phi(CO_2)_{S(my)\text{-sil}}$, and from carbonates, $\phi(CO_2)_{S(my)\text{-carb}}$, were estimated considering the two scenarios and are reported in Table 8. In the silicate-sandstone scenario, $\phi(CO_2)_{S(my)\text{-sil}}$ values were estimated considering the weathering of "sandstone" and "claystone," while $\phi(CO_2)_{S(my)\text{-carb}}$ values were estimated considering the weathering of "pure carbonate" and "mixed carbonate." In the carbonate-sandstone scenario, $\phi(CO_2)_{S(my)\text{-sil}}$

TABLE 8. FLUXES OF ATMOSPHERIC CO_2 CONSUMED BY CHEMICAL WEATHERING COMING FROM SILICATE, $\Phi(CO_2)_{S(my)\text{-sil}}$, AND FROM CARBONATE, $\Phi(CO_2)_{S(my)\text{-carb}}$, WEATHERING EXPRESSED IN MOL KM^{-2} YR^{-1} AND IN PERCENTAGE (%)

Basin ID	River name	Silicate-sandstone scenario				Carbonate-sandstone scenario			
		$\Phi(CO_2)_{S(my)\text{-sil}}$ (mol km^{-2} yr^{-1})	$\Phi(CO_2)_{S(my)\text{-carb}}$ (mol km^{-2} yr^{-1})	$\Phi(CO_2)_{S(my)\text{-sil}}$ (%)	$\Phi(CO_2)_{S(my)\text{-carb}}$ (%)	$\Phi(CO_2)_{S(my)\text{-sil}}$ (mol km^{-2} yr^{-1})	$\Phi(CO_2)_{S(my)\text{-carb}}$ (mol km^{-2} yr^{-1})	$\Phi(CO_2)_{S(my)\text{-sil}}$ (%)	$\Phi(CO_2)_{S(my)\text{-carb}}$ (%)
1	Roia	5.27×10^5	5.04×10^5	51.11	48.89	1.22×10^4	7.61×10^5	1.58	98.42
2	Mella	1.48×10^6	3.67×10^5	80.14	19.86	4.99×10^4	1.08×10^6	4.41	95.59
3	Brenta	5.95×10^5	1.15×10^6	34.02	65.98	0.00	1.45×10^6	0.00	100.00
4	Isonzo	1.83×10^6	3.43×10^6	34.81	65.19	0.00	4.34×10^6	0.00	100.00
5	Livenza	1.58×10^6	4.71×10^5	76.98	23.02	1.77×10^2	1.26×10^6	0.01	99.99
6	Iller	1.18×10^6	4.12×10^5	63.66	22.19	1.35×10^4	9.96×10^5	1.06	78.29
7	Oglio	1.53×10^6	3.06×10^5	83.31	16.69	2.58×10^5	9.40×10^5	21.56	78.44
8	Sesia	2.22×10^6	1.41×10^4	99.37	0.63	3.77×10^5	9.36×10^5	28.71	71.29
9	Tagliamento	9.40×10^5	1.04×10^6	47.51	52.49	5.28×10^3	1.51×10^6	0.35	99.65
10	Var	1.57×10^5	3.87×10^5	28.89	71.11	7.75×10^3	4.62×10^5	1.65	98.35
11	Mincio	6.21×10^4	7.06×10^4	46.79	53.21	4.26×10^3	9.95×10^4	4.10	95.90
12	Lech	1.80×10^6	7.96×10^5	60.69	26.84	2.42×10^4	1.68×10^6	1.17	80.99
13	Enns	9.28×10^5	4.15×10^5	69.07	30.93	3.02×10^5	7.28×10^5	29.32	70.68
14	Mur	5.52×10^5	1.09×10^5	83.55	16.45	3.58×10^5	2.06×10^5	63.49	36.51
15	Dora Baltea	7.01×10^5	1.99×10^5	77.85	22.15	3.35×10^5	3.83×10^5	46.67	53.33
16	Piave	3.80×10^5	3.95×10^5	49.02	50.98	4.99×10^3	5.82×10^5	0.85	99.15
17	Adda	1.36×10^6	2.90×10^5	82.43	17.57	3.96×10^5	7.72×10^5	33.92	66.08
18	Ticino	1.01×10^6	1.15×10^5	89.78	10.22	4.05×10^5	4.19×10^5	49.11	50.89
19	Isar	4.11×10^5	1.02×10^5	50.52	12.54	1.10×10^4	3.02×10^5	1.80	49.22
20	Tanaro	9.31×10^5	2.37×10^5	79.71	20.29	2.01×10^4	6.93×10^5	2.81	97.19
21	Sava	9.64×10^5	9.72×10^5	49.80	50.20	2.95×10^4	1.44×10^6	2.01	97.99
22	Po	1.09×10^6	1.40×10^5	88.59	11.41	8.88×10^4	6.39×10^5	12.19	87.81
23	Adige	5.93×10^5	3.01×10^5	66.34	33.66	2.19×10^5	4.88×10^5	30.98	69.02
24	Drau	8.46×10^5	3.67×10^5	69.77	30.23	3.53×10^5	6.14×10^5	36.51	63.49
25	Rhone	1.08×10^6	3.34×10^5	76.29	23.71	1.73×10^5	7.86×10^5	18.06	81.94
26	Isere	5.74×10^5	4.46×10^5	56.29	43.71	1.63×10^5	6.51×10^5	20.01	79.99
27	Durance	3.26×10^4	4.47×10^4	42.14	57.86	6.47×10^3	5.77×10^4	10.07	89.93
28	Inn	1.13×10^6	3.51×10^5	70.27	21.81	1.58×10^5	8.38×10^5	14.04	74.61
29	Rhine	1.13×10^6	4.29×10^5	69.35	26.29	6.24×10^4	9.63×10^5	5.69	87.83
30	Linth*	1.57×10^6	7.45×10^5	67.81	32.19	1.50×10^5	1.45×10^6	9.35	90.65
31	Reuss*	1.28×10^6	7.84×10^5	62.03	37.97	1.48×10^5	1.35×10^6	9.85	90.15
32	Alpine Rhine*	1.06×10^6	6.08×10^5	63.53	36.47	1.62×10^5	1.06×10^6	13.27	86.73
33	Aare*	6.68×10^5	3.71×10^5	64.29	35.71	1.22×10^4	7.61×10^5	4.19	95.84
	Mean	*9.75×10^5*	*5.06×10^5*	*64.72*	*32.89*	*1.31×10^5*	*9.28×10^5*	*14.64*	*82.30*

Note: The fluxes were estimated considering "sandstone" composed mainly by silicate rocks (silicate-sandstone scenario) and mainly by carbonate rocks (carbonate-sandstone scenario).

*Indicates Rhine subbasins that were sampled only in winter season.

values were estimated considering only the weathering of "claystone," while $\phi(CO_2)_{S(my)\text{-carb}}$ values were estimated considering the weathering of "pure carbonate," "mixed carbonate," and "sandstone." The relative percentages of $\phi(CO_2)_{S(my)\text{-sil}}$ and of $\phi(CO_2)_{S(my)\text{-carb}}$ for the two scenarios were estimated with respect to the total $\phi(CO_2)_{S(my)}$. Table 8 shows that, considering the silicate-sandstone scenario, the contribution of silicate weathering is: (1) between 25% and 50% for eight river basins (Var, Brenta, Isonzo, Durance, Mincio, Tagliamento, Piave, and Sava), (2) between 50% and 75% for 14 river basins (Isar, Roia, Isere, Lech, Reuss, Alpine Rhine, Iller, Aare, Adige, Linth, Enns, Rhine, Drau, and Inn), and (3) between 75% to 100% for 11 river basins (Rhone, Livenza, Dora Baltea, Tanaro, Mella, Adda, Oglio, Mur, Po, Ticino, and Sesia).

Considering the carbonate-sandstone scenario, the contribution of silicate weathering decreases significantly, being: (1) between 0% to 25% for 25 river basins (Brenta, Isonzo, Livenza, Tagliamento, Piave, Iller, Lech, Roia, Var, Isar, Sava, Tanaro, Mincio, Aare, Mella, Rhine, Linth, Reuss, Durance, Po, Alpine Rhine, Inn, Rhone, Isere, and Oglio), (2) between 25% to 50% for seven river basins (Sesia, Enns, Adige, Adda, Drau, Dora Baltea, and Ticino), and (3) between 50% and 75% for one river basin (Mur).

DISCUSSION

The principal aims of this work were: (1) to investigate the relationship between the lithological composition of the main Alpine river basins and their water alkalinity, and (2) to provide generic mathematical parameters that link lithology to the moles of atmospheric CO_2 consumed by chemical weathering.

Elaboration of the Alpine-Geo-LiM

Assuming that the chemical reactions occurring within the basins are those reported in Equations 1–6, the lithological classes of Alpine-Geo-LiM were chosen by considering the mineralogic composition of outcropping rocks. For this reason, metamorphic rocks were classified according to the chemistry of protoliths, and all the rocks for which data on protoliths were unavailable or unclear (e.g., in the case of migmatite, mylonite, and metasediments) were included in the class "metamorphic rocks" (which occupies 1.81% of the whole study area). This criterion represents a novel feature when compared with other global lithologic maps (Gibbs and Kump, 1994; Amiotte-Suchet and Probst, 1995; Amiotte-Suchet at al., 2003; Dürr et al., 2005; Hartmann and Moosdorf, 2012; Moosdorf et al., 2010), where lithologies with very different behavior in the atmospheric CO_2 consumption processes were included in the generic "metamorphic" class. This is the case, for example, of marble, a metamorphic rock composed of carbonate minerals highly prone to consuming atmospheric CO_2. Marble has a very different behavior with respect to other metamorphic rocks, such as, for example, orthogneiss, which is a metamorphic rock derived from a granite/rhyolite protolith that is much less prone to consuming atmospheric CO_2 with respect to marble. The classification of metamorphic rocks according to the chemistry of their protoliths is of particular interest as regards the Alpine chain, where, considering the global lithological map GLiM elaborated by Hartmann and Moosdorf (2012), metamorphic rocks are quite abundant, representing 25.84% of the whole area.

Another novel feature of this work is the release of the map with the procedures (GIS commands and database queries) used to produce the map. We decided to share this information to allow reproducibility and replicability of the research and following the concept of open science (Nüst et al., 2018).

Looking to Alpine-Geo-LiM, it shows that carbonate rocks are the most abundant type in the Alpine region (44.57%), followed by "sandstone" (26.99%), "claystone" (12.87%), "volcanic rocks" (10.50%), "metamorphic rocks" (1.81%), "peats" (0.48%), and "gypsum evaporite" (0.08%). A small area (2.69%) is covered by "water" in the form of lakes and glaciers. The effort in discriminating metamorphic rocks according to the chemistry of protoliths in Alpine-Geo-LiM is demonstrated by the fact that almost all the metamorphic rocks outcropping in the study area (25.84% according to Hartmann and Moosdorf, 2012) were assigned to a specific rock category, and only 1.81% of the study area remains in the general "metamorphic rock" category, used only when information on protoliths was unavailable or unclear.

Overall, the map highlights the presence of an inner core mainly composed of crystalline silicate rocks, bounded to the north and south by rocks mainly composed of carbonates, and finally the presence of rocks composed of sandstones in the basins external to the Alpine chain, coherent with studies by Donnini et al. (2016) and Rossi and Donnini (2018).

Relationship between Basin Lithologies and River Alkalinities

To investigate the relationship between lithological composition of river basins and their water alkalinity, three linear multiple regression analyses were performed following an approach derived from Hartmann et al. (2009); see Equation 11 herein. The first analysis used the linear multiple (*lm*) regression analysis tool (R Core Team, 2016) and considered the original 10 lithological classes of Alpine-Geo-LiM (Table 2). Due to the scarce presence of some lithologies, the other two analyses were performed using the linear multiple (*lm*) and the multiple nonnegative linear (*nnl*) regression analysis (R Core Team, 2016), and considering four lithological classes ("sandstone," "claystone," "total carbonate," and "igneous and metamorphic rocks").

The *b* values obtained from the *nnl* regression analysis (Table 6) were compared with values from literature that considered monolithological basins (Bluth and Kump, 1994; Amiotte-Suchet et al., 2003), and that considered multilithological basins (Hartmann, 2009). The comparison shows that, in the present work, the calibration parameter *b* for "total carbonate" (2.45×10^{-3} mol l^{-1}) is included among the range of literature values (1×10^{-3} to 8×10^{-4} mol L^{-1}), as well as for "claystone," with an estimated *b* value equal to 6.30×10^{-4} mol L^{-1}, i.e., of the same order of magnitude of literature values ranging from 2×10^{-4} to 9×10^{-4} mol L^{-1}. Conversely, the comparison also shows that the estimated *b* value for "sandstone" (4.50×10^{-3} mol L^{-1}) is noticeably higher than literature values (6×10^{-4} to 6×10^{-5} mol L^{-1}). Moreover, the *b* values obtained for the "sandstone" class are always larger than those calculated for "pure carbonate," "mixed carbonate," and "total carbonate" (see Tables 5 and 6). This large discrepancy is explained by the aforementioned cluster analysis (Table 3) results, highlighting that, in the study area, the "sandstone" class is probably composed by a relevant carbonate component. The presence of a relevant carbonate component in the Alpine forelands is explained in Appendix A, and it is well noted in the literature (see, e.g., for the Molasse Basin: Schlunegger et al., 1994, 1998; Kempf et al., 1999; Anne et al., 2017; Abdul Aziz et al., 2008; e.g., for the Po Valley and Adriatic foreland: Fontana et al., 2014). The high *b* value of the "sandstone" class can be also explained with the inclusion of recent alluvial sediments in the "sandstone" class. Besides the weathering acting at the soil-air interface, in fact, they are also exposed to chemical dissolution due to groundwater, which contributes to the basin streamflow. Furthermore, in alluvial sediments, which are usually located in flat and low-elevation areas, the resident time of water in the soil-air interface increases, facilitating the chemical dissolution processes. The presence of large amounts of alluvial sediments in the "sandstone" class is evident from the analysis of Table 1. "Sandstone" slope and elevation mean values are indeed much lower than those observed in the other lithologies. Therefore, results show that

carbonates (in the three forms of "pure carbonate," "mixed carbonate," and "total carbonate"), as expected, have a strong positive correlation with water alkalinity. Surprisingly, the results also show that the correlation is even stronger for "sandstone." This fact can be explained considering that (1) the "sandstone" class includes cemented and uncemented deposits also composed by gravel and sand-carbonate sediments, and, (2) in the analyzed basins, "sandstone" is prevalent (Table 3) in association with "pure carbonate" and "mixed carbonate" rocks.

Interestingly, the "claystone" class (outcropping in ~13% of the area) always shows a positive correlation with water alkalinity; however, depending on the type of regression, it can be low (10 lithological classes, *lm*; 4 classes, *nml*) or high (4 classes, *lm*). The significance associated with the value of the coefficients is low, apart from the medium value estimated by the 4 classes *lm* regression. We explain such behavior with the presence in the study area of other carbonate-rich lithologies that hide the "claystone" influence on CO_2 consumption. Moreover, we observe that the positive values of the *b* coefficient for "claystone" can be due not only to silicate weathering, but also to the chemical dissolution of carbonates that can be present in the "claystone" class rocks.

"Igneous and metamorphic rocks" are scarcely represented in the area (~11%), and their correlation with water alkalinity is always negative or equal to zero (see Tables 5 and 6). The significance of the "igneous and metamorphic rocks" coefficients is generally very low; it is also low in the case of the 4 classes *lm* regression, where it results in medium significance, where the corresponding *P value* is larger than those obtained for the other coefficients. Consequently, the present study shows a negligible contribution of volcanic rocks (acid, mafic, and intermediate) to atmospheric CO_2 consumption. On the contrary, in the literature, it is shown that these lithologies, with *b* values ranging from 1.5×10^{-4} to 4.5×10^{-6} mol L^{-1}, do provide a contribution (even if small) to atmospheric CO_2 consumption. This different behavior is due, of course, to the fact that volcanic rocks constituted by silicate minerals occupy a small percentage (~10%) of the whole study area. Moreover, we maintain that the negative or zero *b* values for the "igneous and metamorphic rocks" class (see Table 6) is due to the fact that *b* was estimated in basins where these lithologies are associated with more abundant carbonate minerals, which are more soluble than silicates (Table 2). This is different from what was done (1) by Bluth and Kump (1994) and Amiotte-Suchet et al. (2003), who considered monolithological basins, and (2) by Hartmann (2009), who considered multilithological basins, but who excluded basins containing more than 0.05% of carbonate sedimentary rocks.

Regarding the "metamorphic rocks" class, the result (very low significance level; see Table 5) is different from the outcomes of other authors (Bluth and Kump, 1994; Amiotte-Suchet et al., 2003; Hartmann, 2009), which could be explained by the fact that we used our own classification scheme for the definition of the lithological map (made available along with the present manuscript). As an example, we believe that either the inclusion or the exclusion of some types of rocks into the metamorphic class, based on the analysis of the protoliths, can have a relevant influence on the estimation of the contribution of this class to the CO_2 consumption. We conclude that, in this study area, these lithologies ("igneous and metamorphic rocks") do not significantly contribute to the atmospheric CO_2 consumption process.

Atmospheric CO_2 Consumption in Alpine Basins

Considering Equation 9, the amount of atmospheric CO_2 consumed by chemical weathering can be estimated starting from river water alkalinity. For this reason, the calibration parameter *b* of Equation 11 expresses the capability of different lithologies to consume atmospheric CO_2 by chemical weathering (high value of *b* corresponds to high capability to consume atmospheric CO_2). Consequently, the analysis shows that the lithologies more prone to consume atmospheric CO_2 are, from the higher to the lower: "sandstone," "carbonates," and "claystone," while the contribution of "igneous and metamorphic rocks" is negligible.

Finally, we applied Equation 12 to estimate the fluxes of atmospheric CO_2 consumed by chemical weathering in the "short-term," $\phi(CO_2)_{short}$, within the study area. The fluxes were calculated considering "sandstone" composed (1) mainly by silicate rocks (silicate-sandstone scenario) and (2) mainly by carbonate rocks (carbonate-sandstone scenario). In Equation 12, we considered the *b* values obtained from the *lm* regression analysis performed using 10 lithologies (see Table 5). For "gypsum evaporites," "metamorphic rocks," "mafic rocks," "acid rocks," and "intermediate rocks," where the *Significance level* of the *b* values was very low (see Table 5), we considered *b* equal to 0. In the silicate-sandstone scenario, the *a* parameter was considered equal to 0.5 for "pure carbonate" and "mixed carbonate" categories and 1 for the remaining rock categories. In the carbonate-sandstone scenario, the *a* parameter was considered equal to 0.5 for "pure carbonate," "mixed carbonate," and "sandstone" categories and 1 for the remaining rock categories. Runoff values (*RO* in Eq. 12) were estimated considering the daily discharge at the time of the two sampling campaigns (in spring season and in winter season) and considering the mean annual discharge, $Q_{(s)}$, $Q_{(w)}$, and $Q_{(my)}$ in Table 4.

As expected, in the carbonate-sandstone scenario, the $\phi(CO_2)_{short}$ values were systematically lower than in the silicate-sandstone scenario, since the *a* parameter for "sandstone" for this scenario was considered equal to 0.5, in contrast to the carbonate-sandstone scenario, where the *a* parameter was considered equal to 1. The percentage difference between the mean annual fluxes estimated considering the carbonate-sandstone scenario and the silicate-weathering scenario (see Eq. 10) was on average 26.99%, with the minimum value of –41.25% for Sesia and the maximum value of –13.74% for Var (see Table 7).

A comparison between the contribution (1) of silicate weathering, $\phi(CO_2)_{S(my)\text{-sil}}$, and (2) of carbonate weathering, $\phi(CO_2)_{S(my)\text{-carb}}$, in the two scenarios (silicate-sandstone and carbonate-sandstone scenarios) is shown in Table 8. As expected, the table shows that considering the carbonate-sandstone scenario, the contribution of silicate weathering is 14.51% of the total $\phi(CO_2)_{S(my)}$, and it increases up to 64.72% in the silicate-sandstone scenario. It is evident that the contribution of $\phi(CO_2)$ from silicates is really dependent on the assumptions made about the chemical composition of the sandstone rocks. In the present work, the results indicate that, in the study area, the sandstone rocks contain a relevant component of carbonate rocks. The general implication of our results is that the estimation of CO_2 consumption in areas where sandstone rocks are relatively abundant cannot be made without a careful evaluation of the carbonate content of the lithotypes that were included in the sandstone class. As a consequence, attention should be paid to the choice of the coefficients adopted from the literature (for the "sandstone" class) for calculating the CO_2 fluxes in any given area different from the areas used for the calibration of the parameters themselves.

The approach here presented is valid in non-polluted areas, for temperate climates, and for lithologies without pyrite (see "Weathering Estimation" section). The absence of pyrite is important because, as highlighted, for example, by Moon et al. (2007), pyrite oxidation generates sulfuric acid, which could weather surrounding carbonate and silicate minerals. Since atmospheric CO_2 is not consumed in this process, not considering pyrite oxidation could lead to an overestimation of the atmospheric CO_2 consumption by silicate weathering. Since both pyrite oxidation and gypsum dissolution lead to

an increase of SO_4^- in river waters (e.g., Berner and Berner, 1996), distinguishing between the gypsum and pyrite sources of SO_4^- in river waters is important for a reliable estimation of the fluxes of atmospheric CO_2 consumed by chemical weathering (Moon et al., 2007). We know that the presence of pyrite in the Alps is well documented (e.g., Kappler and Zeeh, 2000; Lavrič and Spangenberg, 2003; Rantitsch, 2007; Gainon et al., 2007; Grachev et al., 2008; Bernard et al., 2010; Herlec et al., 2010; Sanders et al., 2010; Sabatino et al., 2011; Pálfy and Zajzon, 2012). In addition, in the river waters sampled by Donnini et al. (2016), the samples with a relevant sulfate enrichment were located in the southwest French Alps (Roia, Var, Isere, Durance) and in the southeastern Italian Alps (Tagliamento). Since the presence of gypsum in Triassic carbonate rocks is well documented both in the southwest French Alps (e.g., Olivier et al., 2009) and in the southeastern Italian Alps (e.g., Stefanini, 1976; Longinelli and Flora, 2007), we think that it is more reasonable to consider the SO_4^- enrichment in these river waters as a consequence of evaporite dissolution, rather than pyrite oxidation. For this reason, we maintain that our simplification—which considers the pyrite oxidation negligible—could lead to only a slight overestimation of atmospheric CO_2 consumption.

Global Carbon Cycle Implications

A comparison of the fluxes of atmospheric CO_2 fixed by chemical weathering obtained in this work with those available from the literature shows that minor differences exist at regional scale. In particular, a comparison of the $\phi(CO_2)_{short}$ values obtained in the present work with the $\phi(CO_2)_{short}$ values estimated by Donnini et al. (2016) for the same area shows that the range of atmospheric CO_2 fixed by chemical weathering within the 33 main Alpine river basins is quite similar.

In Donnini at al. (2016), during the spring season, $\phi(CO_2)_{short}$ ranges from 2.60×10^4 mol km^{-2} yr^{-2} (Durance) to 2.03×10^6 mol km^{-2} yr^{-2} (Livenza), and during the winter season, $\phi(CO_2)_{short}$ ranges from 2.48×10^4 mol km^{-2} yr^{-2} (Durance) to 2.04×10^6 mol km^{-2} yr^{-2} (Lech).

In this work, during the spring season, in the silicate-weathering scenario, $\phi(CO_2)_{S(s)}$ ranges from 3.93×10^4 mol km^{-2} yr^{-2} (Durance) to 3.71×10^6 mol km^{-2} yr^{-2} (Livenza), and in the carbonate-weathering scenario, it varies from 3.27×10^4 mol km^{-2} yr^{-2} (Durance) to 2.28×10^6 mol km^{-2} yr^{-2} (Livenza). During the winter season, in the silicate-weathering scenario, $\phi(CO_2)_{S(w)}$ ranges from 3.48×10^4 mol km^{-2} yr^{-2} (Durance) to 3.33×10^6 mol km^{-2} yr^{-2} (Lech), and in the carbonate-weathering scenario, it varies from 2.89×10^4 mol km^{-2} yr^{-2} (Durance) to 2.33×10^6 mol km^{-2} yr^{-2} (Lech). Considering the mean annual discharge, in the silicate-weathering scenario, $\phi(CO_2)_{S(my)}$ ranges from 7.73×10^4 mol km^{-2} yr^{-2} (Durance) to 5.26×10^6 mol km^{-2} yr^{-2} (Isonzo), and in the carbonate-weathering scenario, it ranges from 6.24×10^4 mol km^{-2} yr^{-2} (Durance) to 4.34×10^6 mol km^{-2} yr^{-2} (Isonzo).

Overall, the difference between the mean $\phi(CO_2)_{short}$ estimated in the present work, where the mean values of $\phi(CO_2)_{S(s)}$, $\phi(CO_2)_{S(w)}$, and $\phi(CO_2)_{S(my)}$ are 9.43×10^5 mol km^{-2} yr^{-2}, 9.81×10^5 mol km^{-2} yr^{-2}, and 1.52×10^6 mol km^{-2} yr^{-2} in the silicate-weathering scenario, and 6.89×10^5 mol km^{-2} yr^{-2}, 7.05×10^5 mol km^{-2} yr^{-2}, and 1.09×10^6 mol km^{-2} yr^{-2} in the carbonate-weathering scenario, and the mean $\phi(CO_2)_{short}$ estimated by Donnini at al. (2016) ($4.69 \times 10^5 \pm 1.03 \times 10^5$ mol km^{-2} yr^{-2} in spring season, and $5.35 \times 10^5 \pm 0.97 \times 10^5$ mol km^{-2} yr^{-2} in winter season) is less than one order of magnitude.

Quite similar values were estimated by Gaillardet et al. (1999) for the Rhine, Rhone, and Po basins, respectively 5.42×10^5 mol km^{-2} yr^{-2}, 8.56×10^5 mol km^{-2} yr^{-2}, and 1.12×10^6 mol km^{-2} yr^{-2}, showing that the mean $\phi(CO_2)_{short}$ of these three rivers is much higher than the world average CO_2 consumed by chemical weathering (2.46×10^5 mol km^{-2} yr^{-2}) estimated by the same authors.

We maintain that the data-driven estimation of the CO_2 consumption rates in the Alpine region presented here is more objective than the rates estimated using literature values, since the new *b* parameters presented here were obtained using measured data only.

The results of the present study highlight the importance of discriminating rocks according to their mineralogic composition, paying close attention to the presence of minor carbonate components in rock categories usually considered dominated by silicates, like metamorphic rocks, and, as highlighted by Hartmann et al. (2009), like sandstone and shale (in the present work denominated claystone). It is well known, in fact, that these lithologies could contain a small carbonate content (e.g., Jacobson and Blum, 2003; Emberson et al., 2018). The nonnegligible contribution of carbonates to atmospheric CO_2 consumption of silicate-dominated rock categories was stressed by Hartmann et al. (2009, p. 189), who stated that, at global scale, "about 12.6% of the carbonate CO_2 consumption can be attributed to silicate dominated lithological classes." The same authors highlighted that the global contribution of carbonate sedimentary rocks has been overestimated in the past, being ~25% in Hartmann et al. (2009), in contrast to ~40% in Gaillardet et al. (1999), Munhoven (2002), and Amiotte Suchet et al. (2003).

CONCLUSIONS

Alpine-Geo-LiM is a high-resolution (scale 1:1,000,000) geo-lithological map of the Alps. It represents a novel map when compared with published global lithological maps (Gibbs and Kump, 1994; Amiotte-Suchet and Probst, 1995; Amiotte-Suchet at al., 2003; Dürr et al., 2005; Hartmann and Moosdorf, 2012; Moosdorf et al., 2010) for two main reasons. First of all, the lithological classes used to map the study area were chosen by considering the mineralogic composition of the outcropping rocks. Particular attention was paid in discriminating metamorphic rocks, which were classified according to the chemistry of protoliths. The class "metamorphic rocks" included only the rocks for which data on protoliths were unavailable or unclear. The role of different lithologies in atmospheric CO_2 consumption by chemical weathering was estimated by means of a multilithological approach and by applying a linear multiple regression for predicting water alkalinity based on lithologies. The analyses confirmed that carbonates are lithologies highly prone to consuming atmospheric CO_2, as previously stated by several authors (Bluth and Kump, 1994; Amiotte-Suchet et al., 2003; Hartmann, 2009). The present work also shows that the "sandstone" category, which includes quartzite, and also arkose, graywacke, and conglomerate, could have a nonnegligible carbonate component (Garrels and Mackenzie, 1971; Mottana et al., 2009) and play an important role in consuming atmospheric CO_2. Moreover, the linear multiple regression analyses showed that the contribution of igneous rocks in atmospheric CO_2 consumption is negligible.

The second novel feature is that Alpine-Geo-LiM is being released in vector format together with the procedure used for the definition of the map and the original data in order to allow the replicability and reproducibility of the product (see Donnini et al., 2018).

ACKNOWLEDGMENTS

M. Donnini was supported by a grant from the Fondazione Assicurazioni Generali, and A. Zucchini was partially supported by the research projects of Paola Comodi, Francesco Frondini, and Diego Perugini of the Department of Physics and Geology of the University of Perugia.

M. Donnini mainly contributed to application of the geochemical models and to verification of the accuracy of the map with respect to Alpine geology, I. Marchesini mainly contributed to the geographical and statistical operations, and A. Zucchini mainly contributed to the mineralogical-petrographic considerations useful for elaborating the geo-lithological classification of the map. M. Donnini wrote the paper, which I. Marchesini and A. Zucchini then revised internally.

The Alpine geo-lithological map (Alpine-GeoLiM) represents a portion of the Geo-Lithological Map of Central Europe (Geo-LIM), released in GPKG and

in PDF format in Donnini et al. (2018) - https://doi.org/10.5281/zenodo.3530257. Along with the map, we provide: (1) the original national geological maps of Germany, Italy, Slovenia, France, Switzerland, and Austria, used for creating the map; and (2) a script that can be used to replicate the classification and the union of the original maps.

We are grateful to the two reviewers, who significantly contributed to the overall quality of the manuscript.

REFERENCES CITED

Abdul Aziz, H.A., Böhme, M., Rocholl, A., Zwing, A., Prieto, J., Wijbrans, J.R., Heissig, K., and Bachtadse, V., 2008 Integrated stratigraphy and 40Ar/39Ar chronology of the early to middle Miocene Upper Freshwater Molasse in eastern Bavaria (Germany): International Journal of Earth Sciences, v. 97, no. 1, p. 115–134, https://doi.org/10.1007/s00531-006-0166-7.

Amiotte-Suchet, P., 1995, Cycle du carbone, érosion chimique des continents et transferts vers les océans: Persée-Portail des Revues Scientifiques en SHS, v. 97, no. 1, 178 p, https://www.persee.fr/doc/sgeol_0302-2684_1995_mon_97_1.

Amiotte-Suchet, P., and Probst, J.L., 1993a, Flux de CO_2 consommé par altération chimique continentale: Influences du drainage et de la lithologie (CO_2 flux consumed by chemical weathering of continents: Influences of drainage and lithology): Comptes Rendus de l'Académie des Sciences de Paris, ser. II, Mécanique, Physique, Chimie, Astronomie, v. 317, p. 615–622.

Amiotte-Suchet, P., and Probst, J.L., 1993b, Modelling of atmospheric CO_2 consumption by chemical weathering of rocks: Application to the Garonne, Congo and Amazon basins: Chemical Geology, v. 107, no. 3-4, p. 205–210, https://doi.org/10.1016/0009-2541(93)90174-H.

Amiotte-Suchet, P.A., and Probst, J.L., 1995, A global model for present-day atmospheric/soil CO_2 consumption by chemical erosion of continental rocks (GEM-CO_2): Tellus, ser. B, Chemical and Physical Meteorology, v. 47, no. 1-22, p. 273–280, https://doi.org/10.3402/tellusb.v47i1-2.16047.

Amiotte-Suchet, P., and Probst, J.L., 1996, Origines du carbone inorganique dissous dans les eaux de la Garonne. Variations saisonnières et interannuelles (Sources of dissolved inorganic carbon in the Garonne river water. Seasonal and interannual variations): Sciences Géologiques: Bulletins et Mémoires, v. 49, no. 1, p. 101–126, https://doi.org/10.3406/sgeol.1996.1938.

Amiotte-Suchet, P., Probst, J.L., and Ludwig, W., 2003, Worldwide distribution of continental rock lithology: Implications for the atmospheric/soil CO_2 uptake by continental weathering and alkalinity river transport to the oceans: Global Biogeochemical Cycles, v. 17, no. 2, p. 1–14, https://doi.org/10.1029/2002GB001891.

Anders, E., and Ebihara, M., 1982, Solar-system abundances of the elements: Geochimica et Cosmochimica Acta, v. 46, no. 11, p. 2363–2380, https://doi.org/10.1016/0016-7037(82)90208-3.

Anderson, S.P., 2005, Glaciers show direct linkage between erosion rate and chemical weathering fluxes: Geomorphology, v. 67, no. 1-2, p. 147–157, https://doi.org/10.1016/j.geomorph.2004.07.010.

Anderson, S.P., Drever, J.I., and Humphrey, N.F., 1997, Chemical weathering in glacial environments: Geology, v. 25, no. 5, p. 399–402, https://doi.org/10.1130/0091-7613(1997)025≤0399:CWIGE≥2.3.CO;2.

Anne, C., Naki, A., Susan, I.O., Fritz, S., Peter, K.W., Andreas, D., Joachum, K., Meinert, R., and Christian, S., 2017, Timing of early Quaternary gravel accumulation in the Swiss Alpine foreland: Geomorphology, v. 276, p. 71–85, https://doi.org/10.1016/j.geomorph.2016.10.016.

Bas, M. L., Maitre, R. L., Streckeisen, A., Zanettin, B., and IUGS Subcommission on the Systematics of Igneous Rocks, 1986, A chemical classification of volcanic rocks based on the total alkali–silica diagram: Journal of Petrology, v. 27, no. 3, p. 745–750, https://doi.org/10.1093/petrology/27.3.745.

Bashfield, A., and Keim, A., 2011, Continent-wide DEM creation for the European Union, *in* Surveying & Spatial Sciences Institute; International Center for Remote Sensing of Environment; CSIRO (Australia), 34th International Symposium on Remote Sensing of Environment: The GEOSS Era: Towards Operational Environmental Monitoring: Sydney, Australia, p. 10–15.

Bengtsson, G., and Törneman, N., 2004, Dissolved organic carbon dynamics in the peat–streamwater interface: Biogeochemistry, v. 70, no. 1, p. 93–116, https://doi.org/10.1023/B:BIOG.0000049338.81809.7c.

Bernard, S., Benzerara, K., Beyssac, O., and Brown, G.E., Jr., 2010, Multiscale characterization of pyritized plant tissues in blueschist facies metamorphic rocks: Geochimica et Cosmochimica Acta, v. 74, no. 17, p. 5054–5068, https://doi.org/10.1016/j.gca.2010.06.011.

Berner, E.K., and Berner, R.A., 1996, Global Environment: Water, Air, and Geochemical Cycles: Upper Saddle River, New Jersey, Prentice-Hall, 376 p.

Berner, E.K., and Berner, R.A., 2012, Global Environment: Water, Air, and Geochemical Cycles (2nd ed.): Princeton, New Jersey, Princeton University Press, 443 p.

Berner, R.A., 1991, A model for atmospheric CO_2 over Phanerozoic time: American Journal of Science, v. 291, no. 4, p. 339–376, https://doi.org/10.2475/ajs.291.4.339.

Berner, R.A., 1994, GEOCARB II: A revised model of atmospheric CO_2 over Phanerozoic time: American Journal of Science, v. 294, no. 1, p. 56–91, https://doi.org/10.2475/ajs.294.1.56.

Berner, R.A., 2003, The long-term carbon cycle, fossil fuels and atmospheric composition: Nature, v. 426, no. 6964, p. 323–326, https://doi.org/10.1038/nature02131.

Berner, R.A., 2004, The Phanerozoic Carbon Cycle: CO_2 and O_2: Oxford, UK, Oxford University Press, 158 p.

Berner, R.A., 2006, Inclusion of the weathering of volcanic rocks in the GEOCARBSULF model: American Journal of Science, v. 306, no. 5, p. 295–302, https://doi.org/10.2475/05.2006.01.

Berner, R.A., and Kothavala, Z., 2001, GEOCARB III: A revised model of atmospheric CO_2 over Phanerozoic time: American Journal of Science, v. 301, no. 2, p. 182–204, https://doi.org/10.2475/ajs.301.2.182.

Berner, R.A., Lasaga, A.C., and Garrels, R.M., 1983, The carbonate-silicate geochemical cycle and its effect on atmospheric carbon dioxide over the past 100 million years: American Journal of Science, v. 283, p. 641–683, https://doi.org/10.2475/ajs.283.7.641.

BGR (Bundesanstalt für Geowissenschaften und Rohstoffe), 2011, Geologische Karte der Bundesrepublik Deutschland: Hannover, Germany, BGR, scale 1:1,000,000 (GK1000).

Bluth, G.J., and Kump, L.R., 1994, Lithologic and climatologic controls of river chemistry: Geochimica et Cosmochimica Acta, v. 58, no. 10, p. 2341–2359, https://doi.org/10.1016/0016-7037(94)90015-9.

Boeglin, J.L., and Probst, J.L., 1998, Physical and chemical weathering rates and CO_2 consumption in a tropical lateritic environment: The upper Niger basin: Chemical Geology, v. 148, no. 3-4, p. 137–156, https://doi.org/10.1016/S0009-2541(98)00025-4.

Boggs, S., Jr., and Boggs, S., 2009, Petrology of Sedimentary Rocks: Cambridge, UK, Cambridge University Press, 599 p., https://doi.org/10.1017/CBO9780511626487.

Bonomo, R., Capotorti, F., Compagnoni, B., D'ambrogi, C., Di Stefano, R., Galluzzo, F., Graziano, R., Martarelli, L., Pampaloni, M.L., Pantaloni, M., and Ricci, V., 2006, La Nuova Carta Geologica d'Italia (The New Geological Map of Italy): Memorie Descrittive della Carta Geologica d'Italia 71: Firenze (Italy), p. 113–114, scale 1:500,000.

Bracco, F., Gentilli, A., Minelli, A., Solari, M., Stoch, F., and Venanzoni, R., 2004, Mountain peat bogs: Relicts of biodiversity in acid waters, *in* Minelli, A., ed., Italian habitats: Italian Ministry of the Environment and Territory Protection (Ministero dell'Ambiente e della Tutela del Territorio), Friuli Museum of Natural History (Museo Friulano di Storia Naturale), Municipality of Udine (Comune di Udine, Italy), v. 9, 81 p.

Bundesamt für Landestopografie, 2005, Geologische Karte der Schweiz: Wabern, Switzerland, Bundesamt für Landestopografie, scale 1:500,000.

Bureau de Recherches Géologiques et Minières (BRGM), 2003, Carte Géologique de la France (6ème édition révisée): Paris, BRGM, scale 1:1,000,000.

Buser, S., 2010, Geological Map of Slovenia: Ljubljana, Slovenia, Geological Survey of Slovenia, scale 1:250,000.

Carraro, F., and Giardino, M., 2004, Quaternary glaciations in the western Italian Alps—A review, *in* Ehlers, J., and Gibbard, P.L., eds., Quaternary Glaciations Extent and Chronology: Volume 1, Part 1: Europe: Amsterdam, Elsevier, p. 201–208.

Chow, A.T., Tanji, K.K., and Gao, S., 2003, Production of dissolved organic carbon (DOC) and trihalomethane (THM) precursor from peat soils: Water Research, v. 37, no. 18, p. 4475–4485, https://doi.org/10.1016/S0043-1354(03)00437-8.

Clift, P.D., Shimizu, N., Layne, G.D., Blusztajn, J.S., Gaedicke, C., Schluter, H.U., Clark, M.K., and Amjad, S., 2001, Development of the Indus Fan and its significance for the erosional history of the Western Himalaya and Karakoram: Geological Society of America Bulletin, v. 113, no. 8, p. 1039–1051, https://doi.org/10.1130/0016-7606(2001)113≤1039:DOTIFA≥2.0.CO;2.

Cole, J.J., Prairie, Y.T., Caraco, N.F., McDowell, W.H., Tranvik, L.J., Striegl, R.G., Duarte, C.M., Kortelainen, P., Downing, J.A., Middelburg, J.J., and Melack, J., 2007, Plumbing the global carbon cycle: Integrating inland waters into the terrestrial carbon budget: Ecosystems (New York, N.Y.), v. 10, no. 1, p. 172–185, https://doi.org/10.1007/s10021-006-9013-8.

Dal Piaz, G.V., Bistacchi, A., and Massironi, M., 2003, Geological outline of the Alps: Episodes, v. 26, no. 3, p. 175–180, https://doi.org/10.18814/epiiugs/2003/v26i3/004.

DelSontro, T., McGinnis, D.F., Sobek, S., Ostrovsky, I., and Wehrli, B., 2010, Extreme methane emissions from a Swiss hydropower reservoir: Contribution from bubbling sediments: Environmental Science & Technology, v. 44, no. 7, p. 2419–2425, https://doi.org/10.1021/es9031369.

Dessert, C., Dupré, B., Gaillardet, J., François, L.M., and Allegre, C.J., 2003, Basalt weathering laws and the impact of basalt weathering on the global carbon cycle: Chemical Geology, v. 202, no. 3-4, p. 257–273, https://doi.org/10.1016/j.chemgeo.2002.10.001.

Diem, A., Poulsen, T.M., and Veyret, P., 2019, Alps: Encyclopædia Britannica, https://www.britannica.com/place/Alps.

Diem, T., Koch, S., Schwarzenbach, S., Wehrli, B., and Schubert, C.J., 2012, Greenhouse gas emissions (CO_2, CH_4, and N_2O) from several perialpine and alpine hydropower reservoirs by diffusion and loss in turbines: Aquatic Sciences, v. 74, no. 3, p. 619–635, https://doi.org/10.1007/s00027-012-0256-5.

Doglioni, C., 1994, Foredeeps versus subduction zones: Geology, v. 22, no. 3, p. 271–274, https://doi.org/10.1130/0091-7613(1994)022≤0271:FVSZ≥2.3.CO;2.

Donnini, M., Frondini, F., Probst, J.L., Probst, A., Cardellini, C., Marchesini, I., and Guzzetti, F., 2016, Chemical weathering and consumption of atmospheric carbon dioxide in the Alpine region: Global and Planetary Change, v. 136, p. 65–81, https://doi.org/10.1016/j.gloplacha.2015.10.017.

Donnini, M., Marchesini, I., and Zucchini, A., 2018, A new Geo-Lithological Map (Geo-LiM) for Central Europe (Germany, France, Switzerland, Austria, Slovenia, and northern Italy) (Version 1.0) [Data set]: Zenodo, https://doi.org/10.5281/zenodo.3530257 (dataset accessed 02 December 2019).

Dürr, H.H., Meybeck, M., and Dürr, S.H., 2005, Lithologic composition of the Earth's continental surfaces derived from a new digital map emphasizing riverine material transfer: Global Biogeochemical Cycles, v. 19, no. 4, p. 1–22, https://doi.org/10.1029/2005GB002515.

Egger, H., Krenmayer, H.G., Mandl, G.W., Matura, A., Nowotny, A., Pascher, G., Pestal, G., Pistontnik, J., Rockenschaub, M., and Schnabel, W., 1999, Geologische Übersichtskarte der Republik Österreich: Wien, Austria, Geologische Bundesanstalt, scale 1:1,500,000.

Einsele, G., Ratschbacher, L., and Wetzel, A., 1996, The Himalaya-Bengal Fan denudation-accumulation system during the past 20 Ma: The Journal of Geology, v. 104, no. 2, p. 163–184, https://doi.org/10.1086/629812.

Emberson, R., Galy, A., and Hovius, N., 2018, Weathering of reactive mineral phases in landslides acts as a source of carbon dioxide in mountain belts: Journal of Geophysical Research–Earth Surface, v. 123, no. 10, p. 2695–2713, https://doi.org/10.1029/2018JF004672.

European Environmental Agency, 2010. Alps and the impacts of climate change in Europe today: Copenhagen, Denmark, European Environmental Agency, https://www.eea.europa.eu/signals/signals-2010/alps (accessed 2 December 2019).

FAO-UNESCO (Food and Agriculture Organization, U.N. Educational, Scientific, and Cultural Organization), 1971, 1975, 1976, 1978, 1979, 1981, Soil Map of the World, Volumes I–X: Paris, UNESCO Press.

Fontana, A., Mozzi, P., and Marchetti, M., 2014, Alluvial fans and megafans along the southern side of the Alps: Sedimentary Geology, v. 301, p. 150–171, https://doi.org/10.1016/j.sedgeo.2013.09.003.

Frisch, W., 1979, Tectonic progradation and plate tectonic evolution of the Alps: Tectonophysics, v. 60, no. 3-4, p. 121–139, https://doi.org/10.1016/0040-1951(79)90155-0.

Frondini, F., Zucchini, A., and Comodi, P., 2014, Water-rock interactions and trace elements distribution in dolomite aquifers: The Sassolungo and Sella systems (northern Italy): Geochemical Journal, v. 48, no. 3, p. 231–246, https://doi.org/10.2343/geochemj.2.0301.

Gaillardet, J., Dupré, B., Louvat, P., and Allegre, C.J., 1999, Global silicate weathering and CO_2 consumption rates deduced from the chemistry of large rivers: Chemical Geology, v. 159, no. 1-4, p. 3–30, https://doi.org/10.1016/S0009-2541(99)00031-5.

Gainon, F., Goldscheider, N., and Surbeck, H., 2007, Conceptual model for the origin of high radon levels in spring waters—The example of the St. Placidus spring, Grisons, Swiss Alps: Swiss Journal of Geosciences, v. 100, no. 2, p. 251–262, https://doi.org/10.1007/s00015-007-1220-6.

Galy, A., and France-Lanord, C., 1999, Weathering processes in the Ganges–Brahmaputra basin and the riverine alkalinity budget: Chemical Geology, v. 159, no. 1-4, p. 31–60, https://doi.org/10.1016/S0009-2541(99)00033-9.

Gao, Q., Tao, Z., Huang, X., Nan, L., Yu, K., and Wang, Z., 2009, Chemical weathering and CO_2 consumption in the Xijiang River basin, south China: Geomorphology, v. 106, no. 3-4, p. 324–332, https://doi.org/10.1016/j.geomorph.2008.11.010.

Garrels, R.M., and Mackenzie, F.T., 1967, Origin of chemical compositions of some springs and lakes: Advances in Chemistry Series, v. 67, p. 222–242, https://doi.org/10.1021/ba-1967-0067.ch010.

Garrels, R.M., and Mackenzie, F.T., 1971, Evolution of Sedimentary Rocks: New York, Norton, 408 p.

Gibbs, M.T., and Kump, L.R., 1994, Global chemical erosion during the Last Glacial Maximum and the present: Sensitivity to changes in lithology and hydrology: Paleoceanography and Paleoclimatology, v. 9, no. 4, p. 529–543, https://doi.org/10.1029/94PA01009.

Gislason, S.R., and Oelkers, E.H., 2011, Silicate rock weathering and the global carbon cycle, *in* Harmon, R.S., and Parker, A., eds., Frontiers in Geochemistry: Contribution of Geochemistry to the Study of the Earth: Oxford, UK, Blackwell Publishing, p. 84–103.

Gobiet, A., Kotlarski, S., Beniston, M., Heinrich, G., Rajczak, J., and Stoffel, M., 2014, 21st century climate change in the European Alps—A review: The Science of the Total Environment, v. 493, p. 1138–1151, https://doi.org/10.1016/j.scitotenv.2013.07.050.

Goldich, S.S., 1938, A study in rock-weathering: The Journal of Geology, v. 46, no. 1, p. 17–58, https://doi.org/10.1086/624619.

Grachev, A.F., Pechersky, D.M., Borisovskii, S.E., and Tselmovich, V.A., 2008, Magnetic minerals in sediments at the Cretaceous/Paleogene boundary (the Gams section, eastern Alps), Izvestiya: Physics of the Solid Earth, v. 44, no. 10, p. 789–803, https://doi.org/10.1134/S1069351308100078.

Haas, J., Kovács, S., Krystyn, L., and Lein, R., 1995, Significance of Late Permian–Triassic facies zones in terrane reconstructions in the Alpine–North Pannonian domain: Tectonophysics, v. 242, no. 1-2, p. 19–40, https://doi.org/10.1016/0040-1951(94)00157-5.

Hartigan, J.A., and Wong, M.A., 1979, Algorithm AS 136: A k-means clustering algorithm: Journal of the Royal Statistical Society, ser. C, Applied Statistics, v. 28, no. 1, p. 100–108, https://doi.org/10.2307/2346830.

Hartmann, J., 2009, Bicarbonate-fluxes and CO_2-consumption by chemical weathering on the Japanese Archipelago—Application of a multi-lithological model framework: Chemical Geology, v. 265, no. 3-4, p. 237–271, https://doi.org/10.1016/j.chemgeo.2009.03.024.

Hartmann, J., and Moosdorf, N., 2012, The new global lithological map database GLiM: A representation of rock properties at the Earth surface: Geochemistry Geophysics Geosystems, v. 13, no. 12, p. 1–37, https://doi.org/10.1029/2012GC004370.

Hartmann, J., Jansen, N., Dürr, H.H., Kempe, S., and Köhler, P., 2009, Global CO_2-consumption by chemical weathering: What is the contribution of highly active weathering regions?: Global and Planetary Change, v. 69, no. 4, p. 185–194, https://doi.org/10.1016/j.gloplacha.2009.07.007.

Herlec, U., Spangenberg, J.E., and Lavrič, J.V., 2010, Sulfur isotope variations from orebody to hand-specimen scale at the Mežica lead-zinc deposit, Slovenia: A predominantly biogenic pattern: Mineralium Deposita, v. 45, no. 6, p. 531–547, https://doi.org/10.1007/s00126-010-0290-y.

Holland, H.D., 1978, The Chemistry of the Atmosphere and Oceans, Volume 1: New York, Wiley, 351 p.

Huh, Y., 2010, Estimation of atmospheric CO_2 uptake by silicate weathering in the Himalayas and the Tibetan Plateau: A review of existing fluvial geochemical data, ***in*** Clift, P.D., Tada, R., and Zheng, H., eds., Monsoon Evolution and Tectonics—Climate Linkage in Asia: Geological Society [London] Special Publication 342, p. 129–151, https://doi.org/10.1144/SP342.10.

Huttunen, J.T., Alm, J., Liikanen, A., Juutinen, S., Larmola, T., Hammar, T., Silvola, J., and Martikainen, P.J., 2003, Fluxes of methane, carbon dioxide and nitrous oxide in boreal lakes and potential anthropogenic effects on the aquatic greenhouse gas emissions: Chemosphere, v. 52, no. 3, p. 609–621, https://doi.org/10.1016/S0045-6535(03)00243-1.

Jacobson, A.D., and Blum, J.D., 2003, Relationship between mechanical erosion and atmospheric CO_2 consumption in the New Zealand Southern Alps: Geology, v. 31, no. 10, p. 865–868, https://doi.org/10.1130/G19662.1.

Jha, P.K., Tiwari, J., Singh, U.K., Kumar, M., and Subramanian, V., 2009, Chemical weathering and associated CO_2 consumption in the Godavari River basin, India: Chemical Geology, v. 264, no. 1-4, p. 364–374, https://doi.org/10.1016/j.chemgeo.2009.03.025.

Joosten, H., and Clarke, D., 2002, Wise Use of Mires and Peatlands: Saarijärvi, Finland, International Mire Conservation Group and International Peat Society, 304 p.

Kappler, P., and Zeeh, S., 2000, Relationship between fluid flow and faulting in the Alpine realm (Austria, Germany, Italy): Sedimentary Geology, v. 131, no. 3-4, p. 147–162, https://doi.org/10.1016/S0037-0738(99)00135-9.

Kempf, O., Matter, A., Burbank, D.W., and Mange, M., 1999, Depositional and structural evolution of a foreland basin margin in a magnetostratigraphic framework: The eastern Swiss Molasse Basin: International Journal of Earth Sciences, v. 88, no. 2, p. 253–275, https://doi.org/10.1007/s005310050263.

Kump, L.R., Kasting, J.F., and Crane, R.G., 2009, The Earth System (3rd ed.): Upper Saddle River, New Jersey, Prentice Hall, 432 p.

Lavrič, J.V., and Spangenberg, J.E., 2003, Stable isotope (C, O, S) systematics of the mercury mineralization at Idrija, Slovenia: Constraints on fluid source and alteration processes: Mineralium Deposita, v. 38, no. 7, p. 886–899, https://doi.org/10.1007/s00126-003-0377-9.

Li, G., and Elderfield, H., 2013, Evolution of carbon cycle over the past 100 million years: Geochimica et Cosmochimica Acta, v. 103, p. 11–25, https://doi.org/10.1016/j.gca.2012.10.014.

Longinelli, A., and Flora, O., 2007, Isotopic composition of gypsum samples of Permian and Triassic age from the north-eastern Italian Alps: Palaeoenvironmental implications: Chemical Geology, v. 245, no. 3-4, p. 275–284, https://doi.org/10.1016/j.chemgeo.2007.08.009.

Mackenzie, F.T., and Garrels, R.M., 1966, Chemical mass balance between rivers and oceans: American Journal of Science, v. 264, no. 7, p. 507–525, https://doi.org/10.2475/ajs.264.7.507.

Meybeck, M., 1986, Composition chimique des ruisseaux non pollués en France (Chemical composition of headwater streams in France): Sciences Géologiques: Bulletins et Mémoires, v. 39, no. 1, p. 3–77, https://doi.org/10.3406/sgeol.1986.1719.

Meybeck, M., 1987, Global chemical weathering of surficial rocks estimated from river dissolved loads: American Journal of Science, v. 287, no. 5, p. 401–428, https://doi.org/10.2475/ajs.287.5.401.

Middlemost, E.A., 1994, Naming materials in the magma/igneous rock system: Earth-Science Reviews, v. 37, no. 3-4, p. 215–224, https://doi.org/10.1016/0012-8252(94)90029-9.

Moon, S., Huh, Y., Qin, J., and van Pho, N., 2007, Chemical weathering in the Hong (Red) River basin: Rates of silicate weathering and their controlling factors: Geochimica et Cosmochimica Acta, v. 71, no. 6, p. 1411–1430, https://doi.org/10.1016/j.gca.2006.12.004.

Moosdorf, N., Hartmann, J., and Dürr, H.H., 2010, Lithological composition of the North American continent and implications of lithological map resolution for dissolved silica flux modeling: Geochemistry Geophysics Geosystems, v. 11, no. 11, p. 1–18, https://doi.org/10.1029/2010GC003259.

Montes-Hernandez, G., Findling, N., and Renard, F., 2016, Dissolution-precipitation reactions controlling fast formation of dolomite under hydrothermal conditions: Applied Geochemistry, v. 73, p. 169–177, https://doi.org/10.1016/j.apgeochem.2016.08.011.

Morgan, J.W., and Anders, E., 1980, Chemical composition of Earth, Venus, and Mercury: Proceedings of the National Academy of Sciences of the United States of America, v. 77, no. 12, p. 6973–6977, https://doi.org/10.1073/pnas.77.12.6973.

Mortatti, J., and Probst, J.L., 2003, Silicate rock weathering and atmospheric/soil CO_2 uptake in the Amazon Basin estimated from river water geochemistry: Seasonal and spatial variations: Chemical Geology, v. 197, no. 1-4, p. 177–196, https://doi.org/10.1016/S0009-2541(02)00349-2.

Mottana, A., Crespi, R., and Liborio, G., 2009, Minerali e Rocce: Milano, Italy, Illustrati Mondadori, 608 p.

Munhoven, G., 2002, Glacial-interglacial changes of continental weathering: Estimates of the related CO_2 and HCO_3^- flux variations and their uncertainties: Global and Planetary Change, v. 33, no. 1-2, p. 155–176, https://doi.org/10.1016/S0921-8181(02)00068-1.

Neteler, M., and Mitasova, H., 2008, Open Source GIS: A GRASS GIS Approach (3rd ed.): New York, Springer, International Series in Engineering and Computer Science Volume 773, 406 p.

Neteler, M., Bowman, M.H., Landa, M., and Metz, M., 2012, GRASS GIS: A multi-purpose open source GIS: Environmental Modelling & Software, v. 31, p. 124–130, https://doi.org/10.1016/j.envsoft.2011.11.014.

Nüst, D., Granell, C., Hofer, B., Konkol, M., Ostermann, F.O., Sileryte, R., and Cerutti, V., 2018, Reproducible research and GIScience: An evaluation using AGILE conference papers: PeerJ Preprints, v. 6, e26561v1.

Olivier, J.-M., Carrel, G., Lamouroux, N., Dole-Olivier, M.-J., Mallard, F., Bravard, J.-P., and Amoros, C., 2009, The Rhône River Basin, *in* Tockner, K., Robinson, C., and Uehlinger, U., eds., Rivers of Europe: London, Academic Press, p. 247–295, https://doi.org/10.1016/B978-0-12-369449-2.00007-2.

Pálfy, J., and Zajzon, N., 2012, Environmental changes across the Triassic-Jurassic boundary and coeval volcanism inferred from elemental geochemistry and mineralogy in the Kendlbachgraben section (Northern Calcareous Alps, Austria): Earth and Planetary Science Letters, v. 335–336, p. 121–134, https://doi.org/10.1016/j.epsl.2012.01.039.

Paul, F., Frey, H., and Le Bris, R., 2011, A new glacier inventory for the European Alps from Landsat TM scenes of 2003: Challenges and results: Annals of Glaciology, v. 52, no. 59, p. 144–152, https://doi.org/10.3189/172756411799096295.

Perrin, A.S., Probst, A., and Probst, J.L., 2008, Impact of nitrogenous fertilizers on carbonate dissolution in small agricultural catchments: Implications for weathering

CO_2 uptake at regional and global scales: Geochimica et Cosmochimica Acta, v. 72, no. 13, p. 3105–3123, https://doi.org/10.1016/j.gca.2008.04.011.

Pettijohn, F.J., 1957, Sedimentary Rocks, Volume 2: New York, Harper & Brothers, 718 p.

Pfiffner, O.A., 2014, Geology of the Alps: Berne, Germany, John Wiley & Sons, 368 p.

Pighini, S., Ventura, M., Miglietta, F., and Wohlfahrt, G., 2018, Dissolved greenhouse gas concentrations in 40 lakes in the Alpine area: Aquatic Sciences, v. 80, no. 3, p. 32, https://doi.org/10.1007/s00027-018-0583-2.

Probst, J.L., 1992, Geochemistry and hydrology of continental erosion. Mechanisms, actual global balance and fluctuations over the last 500 million years: Persée-Portail des Revues Scientifiques en SHS, v. 94, no. 1, https://www.persee.fr/doc/sgeol_0302-2684_1992_mon_94_1.

Probst, J.L., Mortatti, J., and Tardy, Y., 1994, Carbon river fluxes and weathering CO_2 consumption in the Congo and Amazon River basins: Applied Geochemistry, v. 9, no. 1, p. 1–13, https://doi.org/10.1016/0883-2927(94)90047-7.

Railsback, L.B., 2006, Some Fundamentals of Mineralogy and Geochemistry: www.gly.uga.edu/railsback, 350 p. (last accessed 17 December 2019).

Rantitsch, G., 2007, Robust sequential factor analysis of geochemical data from the Permian–Triassic Gartnerkofel-1 core (southern Alps): The geochemical response to changing paleo-oceanographic conditions in shallow-marine carbonate platforms: Facies, v. 53, no. 1, p. 129–140, https://doi.org/10.1007/s10347-006-0092-y.

Rossi, M., and Donnini, M., 2018, Estimation of regional scale effective infiltration using an open source hydrogeological balance model and free/open data: Environmental Modelling & Software, v. 104, p. 153–170, https://doi.org/10.1016/j.envsoft.2018.03.005.

Roy, S., Gaillardet, J., and Allegre, C.J., 1999, Geochemistry of dissolved and suspended loads of the Seine River, France: Anthropogenic impact, carbonate and silicate weathering: Geochimica et Cosmochimica Acta, v. 63, no. 9, p. 1277–1292, https://doi.org/10.1016/S0016-7037(99)00099-X.

Sabatino, N., Neri, R., Bellanca, A., Jenkyns, H.C., Masetti, D., and Scopelliti, G., 2011, Petrography and high-resolution geochemical records of Lower Jurassic manganese-rich deposits from Monte Mangart, Julian Alps: Palaeogeography, Palaeoclimatology, Palaeoecology, v. 299, no. 1-2, p. 97–109, https://doi.org/10.1016/j.palaeo.2010.10.039.

Sanders, D., Ostermann, M., Brandner, R., and Prager, C., 2010, Meteoric lithification of catastrophic rockslide deposits: Diagenesis and significance: Sedimentary Geology, v. 223, no. 1-2, p. 150–161, https://doi.org/10.1016/j.sedgeo.2009.11.007.

Schlunegger, F., Matter, A., and Mange, M.A., 1994, Alluvial fan sedimentation and structure of the southern Molasse Basin margin, Lake Thun area, Switzerland: Eclogae Geologicae Helvetiae, v. 86, no. 3, p. 717–750.

Schlunegger, F., Slingerland, R., and Matter, A., 1998, Crustal thickening and crustal extension as controls on the evolution of the drainage network of the central Swiss Alps between 30 Ma and the present: Constraints from the stratigraphy of the North Alpine foreland basin and the structural evolution of the Alps: Basin Research, v. 10, no. 2, p. 197–212, https://doi.org/10.1046/j.1365-2117.1998.00063.x.

Schmid, S.M., Fügenschuh, B., Kissling, E., and Schuster, R., 2004, Tectonic map and overall architecture of the Alpine orogen: Eclogae Geologicae Helvetiae, v. 97, no. 1, p. 93–117, https://doi.org/10.1007/s00015-004-1113-x.

Schwalm, M., and Zeitz, J., 2015, Concentrations of dissolved organic carbon in peat soils as influenced by land use and site characteristics—A lysimeter study: Catena, v. 127, p. 72–79, https://doi.org/10.1016/j.catena.2014.12.007.

Selvam, B.P., Lapierre, J.F., Guillemette, F., Voigt, C., Lamprecht, R.E., Biasi, C., Christensen, T.R., Martikainen, P.J., and Berggren, M., 2017, Degradation potentials of dissolved organic carbon (DOC) from thawed permafrost peat: Scientific Reports, v. 7, p. 45811, https://doi.org/10.1038/srep45811.

Stampfli, G.M., Mosar, J., Favre, P., Pillevuit, A., and Vannay, J.C., 2001, Permian–Triassic evolution of the western Tethyan realm: The Neo-Tethys/east Mediterranean basin connection, *in* Ziegler, P.A., Cavazza, W., Robertson, A.H.F., and Crasquin-Soleau, S., eds., Peri-Tethyan Rift/Wrench Basins and Passive Margins: Memoires du Muséum National d'Historie Naturelle, Paris, Peri-Tethys Memoir 6, p. 51–108.

Stefanini, S., 1976, Composizione delle acque fluviali del Friuli-Venezia Giulia durante la fase di magra e di piena dei corsi d'acqua: Quaderni dell'Istituto di Ricerca sulle Acque, v. 28, p. 386–450.

Tardy, Y., 1986, Le Cycle de l'Eau: Climats, Paléoclimats et Géochimie Globale: Paris, Masson, 338 p.

Team, R.C., 2016, R: A language and environment for statistical computing [Internet]: Wien, Austria, R Foundation for Statistical Computing (document freely available on the internet at: http://www. r-project. org2015).

Tranvik, L.J., Downing, J.A., Cotner, J.B., Loiselle, S.A., Striegl, R.G., Ballatore, T.J., Dillon, P., Finlay, K., Fortino, K., Knoll, L.B., Kortelainen, P.L., Kutser, T., Larsen, S., Laurion, I., Leech, D.M., McCallister, S.L., McKnight, D.M., Melack, J.M., Overholt, E., Porter, J.A., Prairie, Y., Renwick, W.H., Roland, F., Sherman, B.S., Schindler, D.W., Sobek, S., Tremblay, A., Vanni, M.J., Verschoor, A.M., von Wachenfeldt, E., and Weyhenmeyer, G.A., 2009, Lakes and reservoirs as regulators of carbon cycling and climate: Limnology and Oceanography, v. 54, no. 6, p. 2298–2314, https://doi.org/10.4319/lo.2009.54.6_part_2.2298.

Tricart, P., 1984, From passive margin to continental collision; a tectonic scenario for the western Alps: American Journal of Science, v. 284, no. 2, p. 97–120, https://doi.org/10.2475/ajs.284.2.97.

Trümpy, R., 1960, Paleotectonic evolution of the central and western Alps: Geological Society of America Bulletin, v. 71, p. 843–908, https://doi.org/10.1130/0016-7606(1960)71[843:PEOTCA]2.0.CO;2.

Viers, J., Oliva, P., Dandurand, J.L., Dupré, B., and Gaillardet, J., 2007, Chemical weathering rates, CO_2 consumption, and control parameters deduced from the chemical composition of rivers, *in* Drever, J.I., Holland, H.D., and Turekian, K.K., eds., Surface and Ground Water, Weathering, and Soils: Amsterdam, Netherlands, Elsevier, Treatise on Geochemistry Volume 5, p. 1–25.

Weingartner, R., Viviroli, D., and Schädler, B., 2007, Water resources in mountain regions: A methodological approach to assess the water balance in a highland-lowland-system: Hydrological Processes: International Journal (Toronto, Ontario), v. 21, no. 5, p. 578–585, https://doi.org/10.1002/hyp.6268.

Wu, W., Xu, S., Yang, J., and Yin, H., 2008, Silicate weathering and CO_2 consumption deduced from the seven Chinese rivers originating in the Qinghai-Tibet Plateau: Chemical Geology, v. 249, no. 3-4, p. 307–320, https://doi.org/10.1016/j.chemgeo.2008.01.025.

Science Editor: Bradley S. Singer
Associate Editor: Anna Bird

Manuscript Received 14 January 2019
Revised Manuscript Received 3 October 2019
Manuscript Accepted 17 December 2019

Printed in the USA